ACS Sustainable Chemistry & Engineering

pubs.acs.org/journal/ascecg

Research Article

Microwave-Based Synthesis of Functional Morphological Variants and Carbon Nanotube-Based Composites of VS_4 for Electrochemical Applications

Kenna L. Salvatore,[#] Sha Tan,[#] Christopher Tang, Joceline Gan, Matthew Licht, Cheng-Hung Lin, Xiao Tong, Yu-chen Karen Chen-Wiegart, Esther S. Takeuchi, Kenneth J. Takeuchi, Amy C. Marschilok, and Stanislaus S. Wong*

Cite This: *ACS Sustainable Chem. Eng.* 2020, 8, 16397−16412

Read Online

ACCESS | Metrics & More | Article Recommendations | Supporting Information

ABSTRACT: A novel facile, fast, and efficient microwave-assisted method was developed to synthesize a number of diverse nanostructured motifs (ranging from nanorods to nanoflowers) of VS_4 along with its associated composite heterostructures, VS_4/multi-walled carbon nanotube (MWNT; i.e., multi-walled carbon nanotubes). In particular, we have probed and correlated the effects of a number of specific experimental variables, including primarily precursor, solvent, temperature, and time. We noted that nanorods formed more readily with $VO(acac)_2$ as the vanadium precursor and *n*-methyl-2-pyrrolidone (NMP) as a polar reaction solvent. By contrast, we determined that hierarchical three-dimensional (3D) nanoflower-like assemblies, ranging in size from 100 to 200 nm in average diameter, could be controllably synthesized by using Na_3VO_4 as the vanadium precursor and an aqueous water: polar solvent mixture as the reaction medium. We also observed that VS_4 disintegrates, when in the presence of either air, solution, or a combination of these environments, and established that the extent of VS_4 nanorod decomposition could be almost fully prevented by storage under nitrogen. From an application's perspective, our VS_4 is electrochemically active and shows behavior, consistent with the literature. In particular, as compared with pristine VS_4 nanorods alone, we observed enhanced electrochemical activity with (i) 3D hierarchical flower-like motifs, (ii) unique necklace-like VS_4 nanorod−MWNT composites, and (iii) samples in which as-prepared VS_4 nanorods had been annealed. Moreover, we found that the rational application of specific physical and chemical processing treatments, such as (i) thermal annealing to improve crystallinity, (ii) the addition of MWNTs to form conductive composites, and (iii) the evolution of morphology from one-dimensional (1D) nanorods to more complex 3D nanoflowers, was favorable to the resulting electrochemical performance with respect to increasing stability and reversibility.

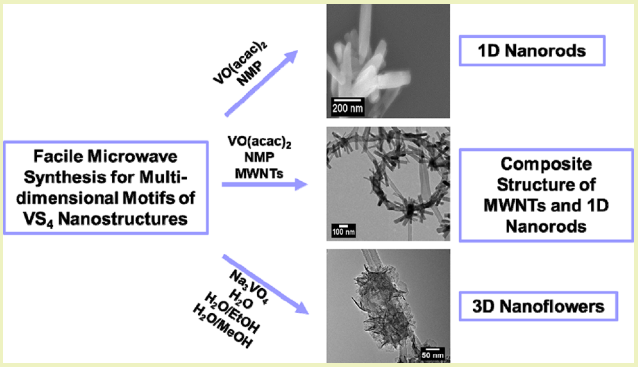

KEYWORDS: *microwave synthesis, scalability, reaction mechanism, carbon nanotube, metal sulfide, electrochemistry*

INTRODUCTION

The development of effective, efficient, and reliable energy storage systems has attracted significant attention in recent years.[1,2] Among such energy storage systems, rechargeable batteries, especially lithium-ion batteries (LIBs), have been studied as viable and promising alternatives, due to their high energy density, long cycling life, and excellent portability.[3,4] Not surprisingly, LIBs have been incorporated as components of not only portable electronic devices but also the underlying powering mechanism behind electric tools and vehicles.

Nevertheless, conventional LIBs incorporating graphite (theoretical capacity of 372 mAh/g) as the anode and $LiCoO_2$ (theoretical capacity of 272 mAh/g) as the cathode, as examples, cannot fully satisfy the increasing demands and aspirational goals of both a higher energy density and a longer cycling life.[5] Recently, transition-metal sulfides have been proposed as an intriguing class of electrode materials. Specifically, due to their (i) reasonable electronic conductivity, (ii) low cost of production, (iii) enviable capability to assume diverse structural motifs, as well as (iv) rich redox chemistry, metal sulfides are appealing, because they can also undergo multi-electron redox reactions, thereby giving rise to a potentially high capacity, which is attractive for their

Received: May 20, 2020
Revised: September 17, 2020
Published: October 28, 2020

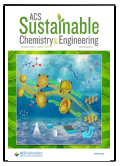

https://dx.doi.org/10.1021/acssuschemeng.0c03785
ACS Sustainable Chem. Eng. 2020, 8, 16397−16412

incorporation within batteries and supercapacitors. As examples of promising higher-capacity electrode materials with moderate conductivity, transition-metal sulfides (FeS_2, CoS_2, and MoS_2) have evinced significant attention for their excellent battery performance.[6−8]

In this manuscript, we focus on VS_4, which is the major component of patronite, a monoclinic prismatic mineral with a linear-chain structure with the space group of $C2/c$. It is composed of V^{4+} ions that are coordinated with sulfur-containing dimeric S_2^{2-} species.[9] Performance-wise, VS_4, when used as an electrode material,[10−19] demonstrates an exceptionally high theoretical capacity of 1196 mAh/g, a finding ascribable not only to its rich redox chemistry and high sulfur content but also to its linear-chain-like structure, which likely facilitates its favorable charge-transfer kinetics, due to weak neighboring-chain interactions.[13] Specifically, its loose stacking structure, constructed from atomic chains held together by weak van der Waals forces and characterized by an interval of 5.83 Å, provides for a number of potential sites for ion insertion/extraction. In addition, VS_4 possesses a narrow band gap (∼1.0 eV), which accounts for its relatively high electronic conductivity.[9] Not surprisingly, VS_4 has been used as a functional electrode material within lithium−sulfur batteries,[20−23] sodium-ion batteries,[24−27] magnesium batteries,[28] aluminum-ion batteries,[29] zinc-ion batteries,[30] and supercapacitors.[31−33] Furthermore, from a catalyst perspective, VS_4 has been utilized[34−37] for both water splitting and dye photodegradation applications.

Despite these numerous advantages, unlike many other binary metal sulfides, work on VS_4 is still comparatively limited, perhaps due to the relative scarcity of reported methods for generating this material. Though VS_4 can be synthesized by heating a mixture of V_2S_3 and sulfur at 400 °C for 4 months,[38] the complex nature of vanadium−sulfur interactions renders it more difficult to obtain a pure stoichiometric product of VS_4 using a more facile method.[39] As such, there are merely two different types of protocols that have been used to successfully generate VS_4, namely (i) solid-state reactions and (ii) hydrothermal/solvothermal reactions. For the solid-state reaction method, heating a mixture of elemental vanadium and sulfur at 400 °C for 10 days can be effective at generating pure products. However, this process still requires a relatively high temperature coupled with long reaction times. The other main (and more practical) method for synthesizing VS_4 involves the use of hydrothermal and solvothermal reactions. In a typical manifestation, Na_3VO_4 and thioacetamide are used as precursors with water as the solvent in the presence of a graphitic template, such as graphene, carbon nanotubes, and so forth.[9] Other groups have improved upon this basic hydrothermal methodology by systematically modifying and optimizing both reaction conditions (e.g., pH) and solvents (e.g., methanol, ethanol, isopropanol, ethylene glycol, etc.) in an attempt to not only devise a template-free method for making VS_4 but also simultaneously create a controllable series of different morphologies of this material, including but not limited to microflowers, nanoscale dendrites, sea-urchin-like structures, and micron-scale spheres.[13,18,35]

Hence, given these limitations on viable choices for creating VS_4, a key objective of our current manuscript has been to develop a milder, solution-based, and relatively facile fabrication alternative. In this regard, microwave-assisted synthesis can achieve very fast reaction times (i.e., minutes) as compared with conventional heating protocols (typically hours), since polar entities (such as solvent water molecules) can directly absorb microwave radiation.[40] Moreover, this technique has been widely applied to nanomaterials' synthesis, such as metals, metal oxides, and metal sulfides. Specifically, the shape, size, crystal structure, and other properties of the desired product can be readily tuned by varying the nature of microwave parameters (i.e., temperature, time, pressure, and power) and associated solvents.[41] As an example, WS_2 incorporating different types of morphologies, including nanocones, nanosheets, and nanoworms, has been obtained simply by altering reaction temperature and precursor concentration.[42] Hence, this relatively fast reaction process coupled with the capability of demonstrating reasonable parameter control renders the microwave-assisted protocol as a viable means for controlling material properties.

As stated previously, VS_4 is a potential electrode material for different battery systems, due to its high theoretical capacity. However, one reason limiting the widespread application of VS_4 in the context of LIBs has been the notable volume expansion observed during Li^+ insertion and extraction, which results in an obvious capacity degradation and a poor rate capability;[13] in fact, severe capacity losses were observed after 50 cycles.[13] Different approaches have been attempted to overcome this problem.

Indeed, as a means of extending the capability and potential of these materials, one workable strategy is to create conductive VS_4-based composites. For instance, VS_4−graphene nanocomposites are excellent candidates when used as LIB anodes, since these can deliver capacity readings of 630 and 314 mAh/g at high rates of 10 and 20 A/g, respectively.[8] VS_4/rGO (reduced graphene), when incorporated as a sodium-ion battery anode material, exhibits a reversible capacity of 362 mAh/g at 100 mA/g.[24] Moreover, VS_4 nanoparticles anchored onto multi-walled carbon nanotubes (MWNTs) delivered 922 mAh/g after 100 cycles at 0.5 A/g, when utilized as an LIB anode.[16] That is, the combination of VS_4 with carbonaceous substances, such as MWNTs, enables the formation of heterostructures, which demonstrate enhanced conductivity for improved charge transfer, desirable mechanical strength to ensure better structural stability, and hence, overall superior activity retention. In general, composites incorporating MWNTs, which are used as an electrode material for lithium-ion batteries, typically exhibit improved metrics in terms of measured energy density, power density, and capacity.[43] As an illustrative example, our team has probed the properties of heterostructures, composed of MWNTs coupled with "zero-strain" $Li_4Ti_5O_{12}$ (LTO) flowers, which had been synthesized by a number of different strategies; this study not only revealed a correlation between preparative treatment and performance but also highlighted the key role of MWNTs in enhancing battery performance.[44] Therefore, to capitalize upon these favorable advantages, we have created VS_4−MWNT composites through an in situ process, by modifying our microwave-based approach.

Rationally designing tailored morphologies denotes a second viable strategy, aimed at addressing the volume expansion issue. For example, nanoscale dendrites of VS_4 with a uniform size of about 300 nm assembled by combining aggregated nanorods with an average individual diameter of about 10 nm[28] were incorporated as a magnesium battery cathode material, and these exhibited an initial discharge capacity of 251 mAh/g at 100 mA/g. In particular, the production of three-dimensional (3D) structural variants of VS_4 nanomateri-

https://dx.doi.org/10.1021/acssuschemeng.0c03785
ACS Sustainable Chem. Eng. 2020, 8, 16397−16412

als is particularly appealing for Li-ion batteries, due to intrinsic morphology-driven benefits, such as (1) greater electron diffusion within the thin constituent two-dimensional (2D) sheets, (2) an increased available surface area allowing for increased numbers of lithiation sites, and (3) a higher degree of porosity, which can potentially accommodate for the characteristic volume change that VS_4 nanomaterials exhibit upon lithiation and delithiation.[18]

Not surprisingly, novel VS_2 nanoflowers have previously been found to exhibit enhanced cyclic stability and improved electrical conductivity as compared with bulk.[45] To explain these observations, it was suggested that a hierarchical 3D nanoscale assembly of constituent VS_2 nanosheets likely leads to better performance by not only reducing overall aggregation but also enhancing the numbers of available active sites and compensating for the inevitable volume change occurring during lithiation.[46] Moreover, in other studies, controlled morphologies of 3D VS_4 nanostructures, ranging from hierarchical micron-scale flowers, octopus-like structures, sea-grass-like motifs, and sea-urchin-like agglomerates, were produced through a facile solvothermal method[18] by systematically varying the nature of the diverse alcohols used in the synthesis process. Among the different kinds of morphologies of VS_4 generated, the sea-urchin-like variant yielded the best performance, when used as an LIB component, as it delivered a capacity of 500 mAh/g at 0.1 A/g. However, comparatively fewer reports have explored the synthesis of template-free 3D VS_4 nanostructures, i.e., the formation of VS_4 in the absence of a carbon template.[18,35] That is, whereas self-assembly[26,47] of smaller component nanostructures, such as nanorods, nanobelts, and nanocones, has been used to generate micron-scale spheres under classical hydrothermal conditions (or variations thereof involving changes in solvent polarity), relatively little if any effort has been expended on the controlled use of microwave synthesis to manufacture 3D nanoscale motifs of VS_4 nanostructures.

Therefore, in this paper, we demonstrate a number of key contributions. First, we developed a new method, i.e., microwave-assisted technique, for successfully synthesizing various VS_4 morphologies (including 3D motifs) in the absence of an underlying template (i.e., carbon). As mentioned, the microwave-assisted method is effective in that it requires a much shorter reaction time to produce pure, monodisperse products with reasonable morphology control as compared with either a conventional hydrothermal/solvothermal method or a solid-state protocol. Key reaction parameters, such as time, solvent, and precursor, are discussed and analyzed in the context of their discrete effect on the resulting morphologies isolated. Second, we have demonstrated that MWNTs can be attached onto VS_4 so as to increase electronic conductivity and structural stability using this microwave-mediated approach. The resulting composite heterostructures incorporating MWNTs consisted of very interesting "necklace"-like motifs. Third, the stability of VS_4 was systematically analyzed for the first time, thereby yielding insights into its possible degradation and decomposition mechanisms with implications for understanding the storage protocols necessary for ensuring their best performance when used as components of batteries and other energy storage media. Fourth, our studies demonstrate favorable structure–property correlations in which electrochemical performance can be rationally tuned through a systematic exploration of both physical and chemical strategies. Specifically, as compared with pristine VS_4 nanorods alone, we observed enhanced electrochemical activity with (i) 3D hierarchical flower-like motifs, (ii) unique necklace-like VS_4 nanorod–MWNT composites, and (iii) samples in which as-prepared VS_4 nanorods had been annealed.

EXPERIMENTAL SECTION

Microwave-Assisted Synthesis of VS_4 Nanorods. The synthesis of VS_4 nanorods was performed using a microwave synthesizer (CEM, Discover SP) instrument, operating using the dynamic mode. First, 0.33 mmol of vanadyl acetylacetonate ($VO(acac)_2$) (Aldrich Chemical Company, 95%) and 1.66 mmol of thioacetamide (TAA) (Alfa Aesar, 99%) were dissolved into a mixture of 4 mL of *n*-methyl-2-pyrrolidone (NMP) (Sigma-Aldrich, 99%) and water (volume (NMP)/volume (deionized (DI) H_2O) = 99.9:0.1) and subsequently sonicated to produce a homogeneous mixture. This solution was subsequently transferred to the microwave reaction vessel (10 mL) followed by a microwave treatment protocol operating at 180 °C for 10 min within a pressure limit of 200 psi and a power threshold of 200 W with medium stirring. After cooling down to room temperature, a resulting black powder was collected by centrifugation and washed with ethanol and water.

Microwave-Assisted Synthesis of 3D Nanostructures of VS_4. The analogous synthesis of VS_4 3D nanostructures was similarly performed using the identical instrument described above, again operating using the dynamic mode. Apart from the reaction temperature, the key difference was in the precursors used. First, 5 mmol of thioacetamide (TAA) (Alfa Aesar, 99%) was dissolved in 14 mL of deionized (DI) water in addition to 10 mL of a specific polar solvent (i.e., water, ethanol, or methanol). Upon complete dissolution, 1 mmol of sodium vanadate (Na_3VO_4) (Aldrich Chemical Company, 95%) was then introduced with subsequent stirring for 30 min to produce a reasonably homogeneous mixture. This solution was then transferred to the microwave reaction vessel (30 mL) for a microwave treatment procedure at 160 °C for 30 min within a pressure limit of 250 psi and a power threshold of 200 W with medium stirring. After cooling down to room temperature, an isolated black powder was collected by centrifugation and washed with ethanol and water.

Synthesis of VS_4 Nanorod (NR)–MWNT Composites. To attach VS_4 nanorods onto MWNTs (SES Research, >95 wt %) through an in situ growth process, a similar method for making pristine VS_4 was utilized. The as-obtained samples of commercial MWNTs that we worked with were characterized by lengths of several microns and average outer diameters, measuring in the range of 40–100 nm. In the first step, set quantities of these MWNTs (~8 mg to ensure a final weight percent of 10%) were added into a mixture of vanadium precursor and sulfur precursor with the assistance of ultrasonication to render them as well-dissolved species, dispersed in solution. Subsequent microwave treatment was conducted at 180 °C for 10 min under identical conditions. Finally, the as-prepared VS_4 nanorod/MWNT composites were separated by centrifugation, following by washing with ethanol and water.

Characterization Methods. *X-ray Diffraction (XRD).* Powder X-ray diffraction has been utilized to analyze the crystallographic information and confirm the chemical composition of as-prepared samples. To prepare the XRD sample for analysis, the product was dispersed in ethanol with sonication and then deposited onto a zero-background holder (MTI Corporation, zero diffraction plate for XRD, B-doped, p-type Si, 23.6 mm in diameter by 2 mm in thickness); the relevant material was air-dried, prior to characterization. The Rigaku Miniflex diffractometer was used to obtain sample powder XRD data, operating in the Bragg configuration with Cu Kα radiation (λ = 1.5418 Å) over the 2θ range of 10–80°, utilizing a scan rate of 15°/min.

Electron Microscopy. Electron microscopy techniques, including scanning electron microscopy (SEM), transmission electron microscopy (TEM), and high-resolution transmission electron microscopy (HRTEM), have been used to characterize and obtain information on sample morphology, sample size, and crystal lattice identification. The

https://dx.doi.org/10.1021/acssuschemeng.0c03785
ACS Sustainable Chem. Eng. 2020, 8, 16397–16412

SEM data were obtained by a Hitachi 4800S instrument under 5 kV voltage conditions. To prepare the SEM sample, the VS_4 powder was sonicated in ethanol for ~30 s to ensure a uniform and homogeneous dispersion, prior to deposition onto a silicon wafer followed by air drying for SEM characterization. The TEM and HRTEM samples were prepared by drop-casting aliquots of a VS_4 suspension in ethanol onto a lacey carbon-coated 300 mesh copper grid. The TEM images were collected using a JEOL JEM 1400 LaB6 TEM, equipped with a 2048 × 2048 Gatan charge-coupled device (CCD) camera, operating at an accelerating voltage of 120 kV. HRTEM analysis was performed on a JEOL 2100F, run with an accelerating voltage of 200 kV.

X-ray Photoelectron Spectroscopy (XPS). X-ray photoelectron spectroscopy was used to confirm elemental composition and derive oxidation state information about the various different elements within our samples. Specifically, XPS sample preparation was similar to that used for SEM. The samples were dispersed in ethanol by sonication for some time and then drop-cast onto a Si wafer (1 cm × 1 cm). The XPS characterization was conducted using a homemade system, with a model SPECS Phoibos 100 electron energy analyzer for electron detection. Al Kα radiation (1486.6 eV) (model XR 50) was used as the X-ray source for the characterization process. Data collected in the V 2p and S 2p regions were interpreted using commercial CasaXps software; we used well-established background correction and curve fitting algorithms for our subsequent data processing.

Electrochemical Analysis. VS_4 electrodes were tape-cast onto copper foil and were characterized by an overall compositional ratio of 80:10:10 in terms of active material, carbon, and poly(vinylidene fluoride) (PVDF) binder by mass. Specifically, the coating composition consisted of 80% active material, 10% Super P carbon, and 10% PVDF. The concentrations of the ink were as follows, for the various samples tested in NMP: VS_4, ~83% of the slurry by mass (remaining 17% is solid) and VS_4/MWNT composite, ~86% of the slurry by mass. After mixing, the resulting slurry was poured onto the copper foil. A "doctor blade" was pulled across the paint/foil to ensure uniformity and the presence of "even" coatings. The material was then dried at 50 °C for over 12 h to remove excess solvent. The corresponding mass loadings (per cm^2) for the electrodes tested, both in terms of overall mass and mass of the active material, were computed to be for (a) VS_4: overall mass, 1.34 mg/cm^2; active, 1.07 mg/cm^2; and (b) VS_4/MWNT: overall mass, 1.26 mg/cm^2; active, 1.01 mg/cm^2.

Stainless steel coin-type cells, possessing a Li foil anode, 1 M $LiPF_6$ in ethylene carbonate/dimethyl carbonate (3:7 vol/vol) electrolyte, and a polypropylene separator, were assembled in an argon-filled glovebox. Cyclic voltammetry measurements were collected using a BioLogic VSP potentiostat over a voltage range of 0.01−3.0 V (note the lower limit of the specific sample indicated in each figure) versus Li/Li^+ at a scan rate of 0.1 mV/s, wherein the lithium metal served as both the counter and reference electrodes.

Synchrotron 3D X-ray Nanotomography. 3D tomography was conducted on as-prepared VS_4 and VS_4/MWNT samples using transmission X-ray microscopy (TXM) at the Full-Field X-ray Imaging Beamline[48] (FXI, 18-ID) of the National Synchrotron Light Source II (NSLS-II) at Brookhaven National Laboratory. To prepare the various samples for the FXI beamline, small amounts of as-prepared VS_4 and composite VS_4/MWNT powders were sealed within a capillary tube using clay, then glued onto a pin using epoxy, and later air-dried for at least 24 h before imaging in TXM. The samples were imaged with an incident X-ray energy of 5.5−6 keV, which was higher than the absorption K-edge of V to optimize the image absorption contrast. The 2D projections of the samples were collected over an angular range of 180° with a total number of projection images of >1500. The projections were then reconstructed using Tomopy.[49] The 3D visualizations of the reconstructed volume were carried out by an open-source software platform, known as Tomviz.[50]

RESULTS AND DISCUSSION

VS_4 Nanorods and VS_4 Nanorod/MWNT Composites. The XRD pattern of as-prepared VS_4 (Figure 1A) corresponds well with the standard monoclinic pattern of VS_4 (JCPDS no. 87-0603), thereby confirming its relatively high purity with no obvious impurities. Morphology was assessed using SEM images of the as-obtained VS_4 sample. In particular, a specimen of VS_4, acquired after a 10 min reaction at 180 °C (Figure 1B) under reaction conditions consisting of a maximum of 200 psi pressure coupled with a threshold of 200 W operating in the dynamic mode, was composed of individual nanorods with average lengths of ~318 nm and corresponding widths of ~77 nm. To the best of our knowledge, nanoscale structures of VS_4 within this size regime have not been routinely reported.

XPS was used to confirm the chemical signature of as-prepared VS_4 nanorods (Figure 1C,D). Specifically, an XPS survey spectrum (Figure S1) was collected for the as-obtained VS_4 sample to acquire information about surface composition and valence states. These data demonstrate the presence of both V and S elements within the sample, with no evident, additional elemental impurities appearing. The V 2p region (Figure 1C) highlights three peaks, located at 515.6, 519.1, and 522.6 eV (Table S1). The peaks situated at 515.6 and 522.6 eV can be assigned to the V $2p_{3/2}$ and V $2p_{1/2}$ states, respectively, suggesting that the oxidation state of V is 4+. In addition, the peak located at 519.1 eV is most likely a vanadium satellite peak.[51] Moreover, there are two peaks, present in the S 2p region (Figure 1D and Table S1); these are located at 162.3 and 163.4 eV corresponding to S_2^{2-}, which maintains a higher binding energy as compared with S^{2-}.[28]

Considering their high conductivity and outstanding mechanical strength, MWNTs were introduced into the reaction mixture under microwave reaction conditions. These experiments yielded a necklace-like heterostructure of a VS_4/MWNT composite, as shown by SEM and TEM images in Figure 1E,F, respectively. The precise mechanism by which our VS_4/MWNT composites formed is a matter of hypothesis. Nonetheless, relevant previous literature has suggested that during the microwave-assisted process, the vanadium precursor is oxidized and forms an initial coating of VO_2 on the external surface of the underlying MWNTs. Subsequently, the reaction of this metal oxide with the sulfur precursor leads to the generation of the observed VS_4 in a stepwise process. It is therefore proposed that the MWNTs act as an underlying structural "backbone" with which to facilitate, guide, and enable the subsequent nucleation and growth of VS_4 nanorods.[52]

According to SEM and TEM images, the VS_4 nanorods within the VS_4/MWNT composite possess similar dimensions to those of isolated, unmodified VS_4, thereby suggesting that the introduction of MWNTs did not perceptibly affect and impact upon VS_4 nanorod growth. High-resolution TEM (HRTEM) images have also been acquired for the composite (Figure 1G,H). The crystalline fringes of the isolated nanorods in Figure 1H are characterized by a lattice plane distance of 0.56 nm, indicative of the (110) planes of monoclinic VS_4.

The corresponding powder XRD pattern (Figure S2) of the VS_4/MWNT composite was consistent with the presence of pure VS_4 coupled with the addition of an extra peak at ~26°, which could be assigned to MWNTs. XPS has also been utilized to analyze VS_4/MWNT heterostructures, as shown in Figure S3. XPS data of both V 2p (Figure S3A) and S 2p

https://dx.doi.org/10.1021/acssuschemeng.0c03785
ACS Sustainable Chem. Eng. 2020, 8, 16397−16412

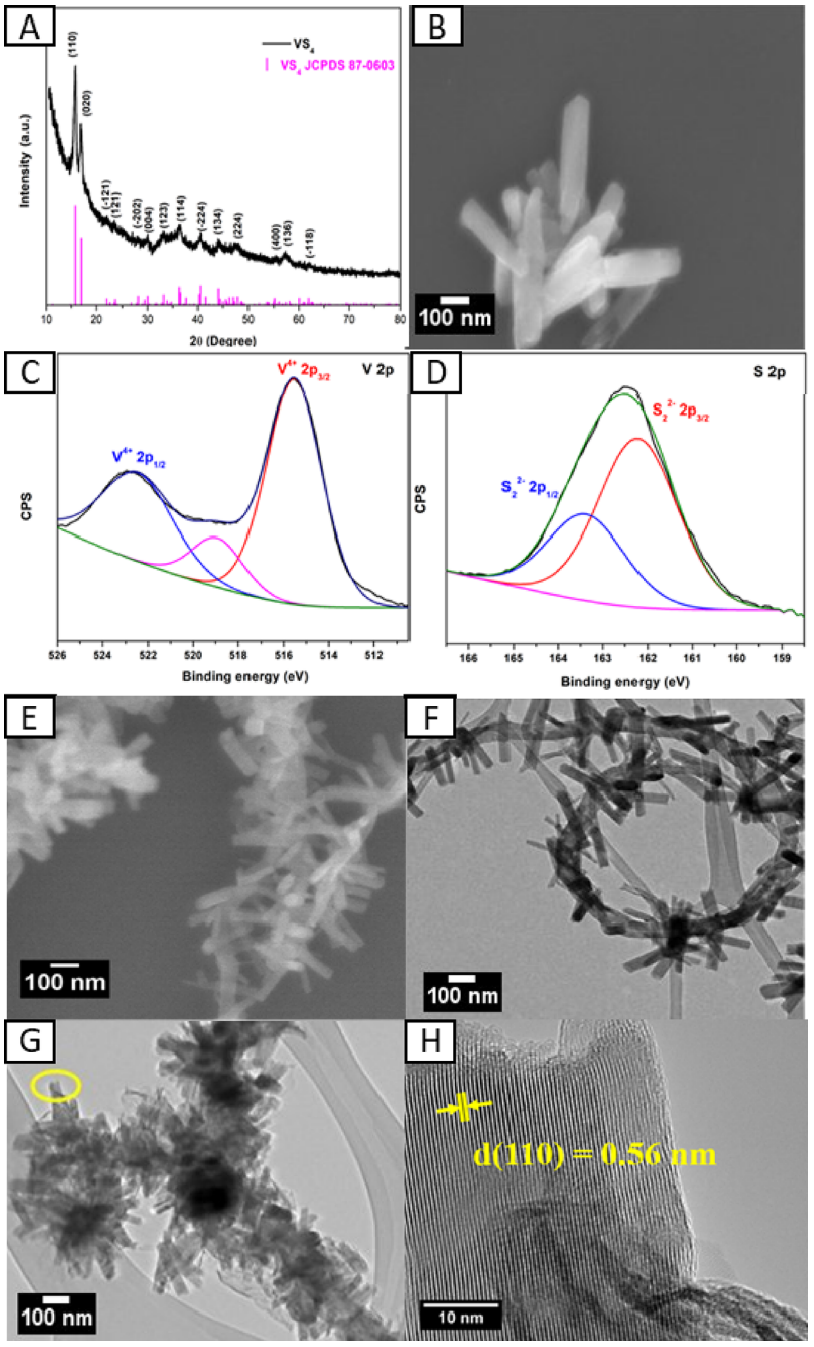

Figure 1. (A) XRD patterns of VS_4 nanorods (black) along with the standard diffraction pattern, i.e., JCPDS no. 87-0603 (purple). (B) SEM image of as-prepared VS_4 nanorods. XPS spectra of as-obtained VS_4 nanorods of (C) the V 2p region and (D) the S 2p region. (E) SEM image, (F) TEM image, and (G, H) HRTEM images of various as-prepared VS_4 nanorod/MWNT composites.

(Figure S3B) signals were similar to those found within the VS_4 sample in the absence of MWNTs, as noted in Table S1. The data confirm the presence of a V^{4+} state coupled with the S_2^{2-} dimer formation. Moreover, after introducing MWNTs into the system, there were two different peaks within the C 1s region (Figure S3C). The peak located at 284.3 eV could be ascribed to a C−C signal, associated with the presence of MWNTs, whereas the peak positioned at 285.7 eV derived from C−O interactions.

Effect of Annealing on Crystallinity of VS_4/MWNT Composites. High-temperature annealing represents a common methodology used for increasing sample crystallinity while simultaneously retaining chemical composition and morphology. Therefore, to enhance the crystallinity of the sample, VS_4/MWNT composites were treated under Ar at 300 °C for 1 h at a ramp rate of 2°/min. The resulting XRD patterns (Figure S4A) of the post-annealed sample evinced sharper peaks, which also matched up well with the standard diffraction pattern, suggesting that the annealing treatment did not introduce any obvious impurities. To investigate if the annealing process impacted upon morphology, SEM images were acquired for the post-annealed sample, as shown in Figure S4B. These data do not reveal any apparent morphological changes; in fact, isolated structures maintained similar dimensions.

https://dx.doi.org/10.1021/acssuschemeng.0c03785
ACS Sustainable Chem. Eng. 2020, 8, 16397−16412

Synthesis Parameter Study and Morphology Control of VS_4. As previously discussed, specific parameters associated with the microwave synthesis process are known to give rise to important consequences with respect to product crystal structures and isolated morphologies. Therefore, to acquire a better understanding of this synthetic algorithm and the underlying mechanism behind this process, the influence of different reaction parameters upon the products formed has been investigated, including but not limited to reaction time and reaction temperature. Indeed, the as-obtained VS_4 morphology could be tuned by simply controllably adjusting these reaction conditions, often at the same time.

Synthesis of VS_4 Nanorods: Varying Reaction Temperature and Reaction Time. Reaction temperature affects the observed crystallinity to a large extent. Therefore, to properly probe the effect of reaction temperature, with other reaction conditions kept constant, the reaction time was set at 10 min. The thermal decomposition temperature of thioacetamide is ~120 °C, a point at which H_2S is released and is able to react with the vanadium precursor to form VS_4 above this temperature.[53] Hence, to analyze the effect of varying reaction temperatures, three different readings above 120 °C were chosen to understand this phenomenon. For example, when the reaction temperature was 140 °C, the product was amorphous with no sharp peaks, observed in the XRD pattern in Figure S5A. It is worth mentioning that nonuniform nanorods were obtained at this temperature, as shown in Figure 2C. With an increase in temperature to 200 °C, peaks attributable to VS_4 appeared, indicative of higher crystallinity, and these not only corresponded well with the standard pattern but also were coupled with the observation of a more uniform product morphology (Figure 2D).

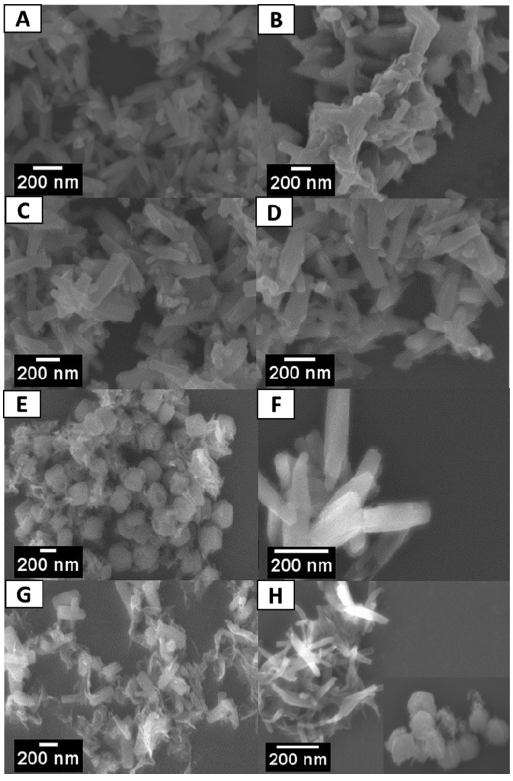

Figure 2. Probing the effect of reaction temperature, reaction time, and solvent of VS_4 nanorod synthesis. SEM images of VS_4 nanorods prepared at 180 °C for (A) 5 min and (B) 15 min and for 10 min at (C) 140 °C and (D) 200 °C. SEM images of VS_4 nanorods, prepared by varying solvent composition: (E) pure NMP; NMP/H_2O (by volume) solution mixtures of (F) 99.9:0.1 and (G) 99.5:0.5; and (H) pure dimethylformamide (DMF).

To study the temporal evolution of VS_4 growth, other reaction conditions were kept the same with the reaction temperature set at 180 °C. The microwave treatment was then conducted for relatively short (but practical) periods of reaction time, i.e., 5, 10, and 15 min in separate experiments. Based on almost identical XRD patterns isolated after these different reaction times (Figure S5B), it was concluded that the reaction time does not dramatically affect chemical composition and degree of crystallinity, presumably because the unique and fast-heating mechanism associated with microwave chemistry invariably leads to the rapid formation of the VS_4 phase within a relatively short time period. However, with respect to the morphology, the 5 min sample (Figure 2A) and 15 min sample (Figure 2B) appeared to be less uniform as compared with the 10 min sample. We hypothesize that under these conditions, the nucleation time for VS_4 formation is too "short" at 5 min but conversely too "long" at 15 min. Nevertheless, as compared with previous synthetic protocols for VS_4, the microwave treatment used herein significantly shortens the necessary reaction time from several hours (and even days) to an interval of mere minutes. All of these runs were performed, without compromising upon either the expected chemical composition or the formation of a homogeneous and uniform product morphology, thereby rendering the entire process both more facile and faster as compared with conventional solid-state and hydrothermal/solvothermal reactions.

Synthesis of VS_4 Nanorods: Varying Sulfur Precursors and Solvents. With respect to the production of hierarchical motifs building on a "starting point" of anisotropic one-dimensional (1D) VS_4 nanorods, we found that a closely integrated convolution of different reaction variables working synergistically together enabled the formation of the desired, high-surface-area structures. Specifically, in addition to the (i) reaction time and (ii) reaction temperature, parameters including (iii) reaction precursors and (iv) solvents were also systematically altered, as well. Nevertheless, it was obvious that the choice of solvent is particularly critical, since the microwave radiation absorbing efficiency and concomitant capability of converting microwave energy into heat are contingent upon the loss tangent of the reaction medium. The higher the loss tangent, the more easily the solvent can absorb microwave energy and convert it into heat.[54] As such, solvents characterized by different loss tangents were tested, and these were shown to have an impact upon not only composition but also morphology.

Varying Sulfur Precursor. As reported previously, the identity of the sulfur source plays an equally important role in sulfide formation, which in and of itself could impact upon the observed morphology and crystallinity, because of correspondingly different decomposition behaviors and sulfur-releasing rates.[55,56] Therefore, we tried out a separate sulfur precursor to analyze its effect upon VS_4 synthesis. For example, in one series of experiments, we replaced TAA (CH_3CSNH_2) with L-cysteine ($HSCH_2CH(NH_2)COOH$), which is also a common sulfur-containing source for synthesizing various types of sulfides. We found that VS_4 could be produced without any obvious impurities, although with much lower crystallinity, as shown in Figure S6Aii.

https://dx.doi.org/10.1021/acssuschemeng.0c03785
ACS Sustainable Chem. Eng. 2020, 8, 16397−16412

Interestingly, the morphology altered from nanorods to amorphous-looking, hierarchical wispy "sheet-like" structural motifs, an observation noted in Figure S6B.

This morphological variant might be attributed to the different decomposition rates of thioacetamide and L-cysteine. Specifically, thioacetamide degrades close to 120 °C, whereas L-cysteine maintains a higher decomposition temperature of around 220 °C.[57] This much higher decomposition temperature for L-cysteine likely leads to a much slower H_2S releasing rate. Our isolated product possessed a lower degree of crystallinity, as evinced by associated XRD data (Figure S6A). In principle, these observations are consistent with a relatively slow nucleation process. We should note that we also tried out thiourea as another potential viable sulfur-containing precursor. However, we were unable to generate the correct composition, likely due to its lower solubility within NMP as compared with either TAA or L-cysteine (Figure S6Ai).

Varying Solvent. The solvent effect with respect to the impact of NMP is summarized in Figure 2E−H. The importance of NMP for the synthesis of VS_2 and VSe_2 cannot be overstated from the literature. Specifically, the high polarity of NMP is necessary to dissolve precursors, and moreover, the surface energy value of NMP is conducive to the formation of "flower-like" structures of VS_2 and VSe_2.[46,58] However, we found that the use of pure NMP in solution in this synthesis was not able to generate a uniform morphology of VS_4; instead, a mixture of nanoscale spheres and nanorods was isolated, as shown in Figure 2E. For these as-obtained nanoscale spheres, they appeared to be composed of individual nanorods, agglomerated together, as shown in Figure S7.

By contrast, when NMP containing a small amount of water was used as the reaction medium, the amount of nanoscale spheres dramatically lessened, whereas the proportion of uniform, discrete nanorods clearly predominated, as shown in Figure 2F. We hypothesize that the presence of water tends to not only promote and favor individual nanorod formation but also prevent their aggregation into sphere-like clusters. Indeed, with increasing water content, it turned out that little if any spherical motifs were generated. Rather, a mixture of nanorods and nanosheets was isolated, as shown in Figure 2G. Nevertheless, it should be noted that when the reaction medium consisted exclusively of water in the presence of $VO(acac)_2$ as the vanadium precursor, no VS_4 crystallized at all, as noted by the corresponding experimental XRD pattern (Figure S8ii). One possible reason for these observations is that the use of water alone cannot completely dissolve the vanadium precursor and, furthermore, water is characterized by a relatively low loss tangent. Hence, running the reaction in water by itself results not only in a slower heating rate but also in a poorer precursor solubility as compared with an NMP/water mixture; these factors can perceptibly affect the dynamics of the microwave reaction itself.

To probe the effect of NMP upon VS_4 synthesis, different polar solvents, namely, *N*,*N*-dimethylformamide (DMF), methanol, and ethanol, were attempted in the synthesis process. The use of DMF resulted in the production of pure VS_4, according to the as-generated XRD pattern (Figure S8i). The associated morphology of VS_4 produced from DMF similarly yielded a mixture of nanoscale spheres and nanorods (Figure 2H). As mentioned previously, the addition of water to the reaction medium may be conducive to the formation of VS_4 nanorods, since as we have seen, the presence of small amounts of water can increase the solubility of the vanadium precursor within the overall solvent environment (such as NMP); consequentially, this scenario would favor not only an increase in the purity of the resulting product but also the generation of a more uniform product morphology. It should be noted, however, that the choice of DMF did not neatly abide by this logic. That is, whereas DMF could create VS_4 in the absence of water, interestingly, DMF in the presence of water yielded little if any product of significance.

The roles of additional polar solvents, such as methanol and anhydrous ethanol, were also investigated with respect to their ability to form VS_4 nanorods. However, it was observed that the vanadyl acetylacetonate precursor did not fully dissolve under these solvent conditions. Indeed, the associated XRD patterns highlight the presence of an impurity peak, suggestive of undissolved precursors (Figure S9i,ii). Upon trying out a

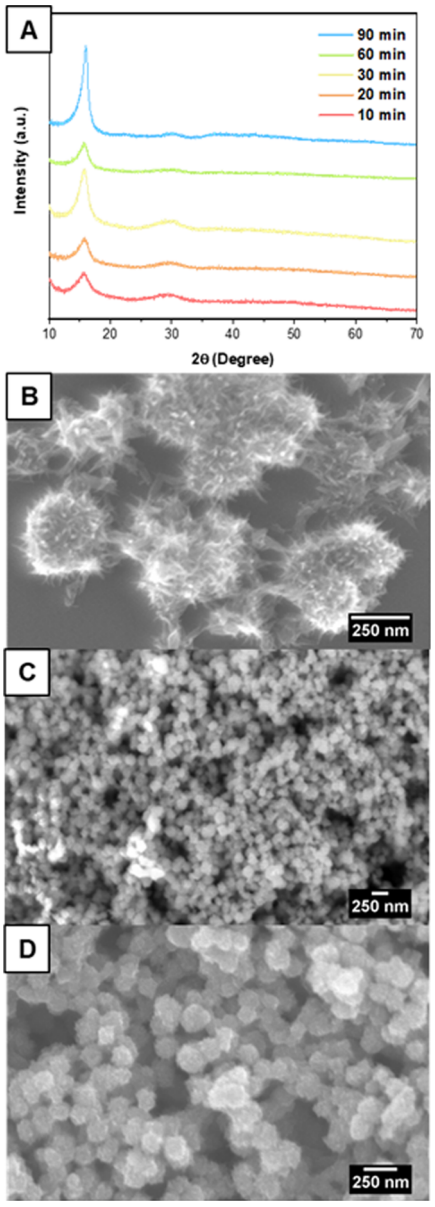

Figure 3. Probing the effect of reaction time in VS_4 nanoflower synthesis. (A) XRD patterns associated with the synthesis of VS_4 using Na_3VO_4 as the vanadium precursor and water as the solvent. Data were collected as a function of increasing reaction time (bottom to top). Representative SEM images of samples at (B) 10 min, (C) 30 min, and (D) 90 min are shown.

https://dx.doi.org/10.1021/acssuschemeng.0c03785
ACS Sustainable Chem. Eng. 2020, 8, 16397−16412

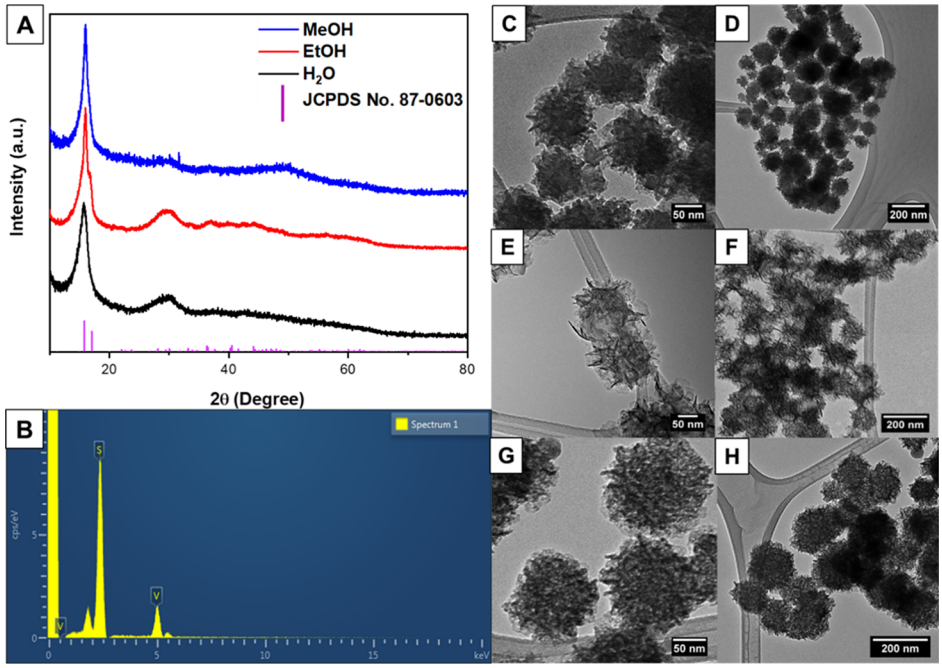

Figure 4. Probing the effect of solvent in VS_4 nanoflower synthesis. (A) XRD patterns of VS_4 3D nanostructures, synthesized using Na_3VO_4 as the vanadium precursor in the presence of water (black), a water/ethanol mixture (red), and a water/methanol mixture (blue), along with a database standard (purple). (B) Representative SEM-EDS spectrum of the VS_4 NF-W sample. Characteristic TEM images of VS_4 3D nanoflowers synthesized in the presence of (C, D) water (NF-W), (E, F) a water/ethanol mixture (NF-E), and (G, H) a water/methanol mixture (NF-M).

mixture of H_2O and either ethanol or methanol (Figure S9iii,iv, respectively), the amounts of dissolved precursors did perceptibly increase but not to a complete extent. In particular, the XRD data indicate that, for the "methanol-and-water" combination, a small but non-negligible amount of remnant precursor lingered, whereas with the "ethanol-and-water" mixture, smaller impurity peaks remained.

Synthesis of 3D Nanostructures of VS_4: Probing the Effects of Reaction Time, Solvent Choice, Sulfur Precursor Concentration, and Order of Reagent Addition. *Varying Reaction Times.* As mentioned in the Introduction section, an example of a typical prior synthesis of 3D nanoflower-like structures of VS_4[18] involved TAA and Na_3VO_4 as the relevant elemental precursors, dissolved in water, in the context of a hydrothermal reaction protocol; at times, these reactions also precipitated unwanted VS_2 as a byproduct. However, the parallel formation of 3D nanostructures of VS_4 within the framework of microwave-assisted reactions is relatively unstudied. Herein, as a key modification of our microwave-assisted reaction conditions described above, we replaced vanadyl acetylacetonate, which we had specifically utilized to promote 1D VS_4 nanorod formation, with sodium orthovanadate (Na_3VO_4), since the latter had previously been reported to be an appropriate and widely utilized source of vanadium for preparing different types of analogous 3D metal sulfides.[51,59,60]

Specifically, we initially analyzed the behavior of sodium orthovanadate in water at varying reaction time periods, i.e., 10 min intervals from 10 to 90 min (Figure 3). In particular, we observed a distinctive increase in crystallinity from 10 to 30 min (Figure 3Ai,ii). However, as the reaction time was further increased from 30 to 60 min and onwards to 90 min, the corresponding improvement in crystallinity was minimal at best (Figure 3Aii,iii). Representative SEM images were taken of samples isolated after 10 min (Figure 3B), 30 min (Figure 3C), and 90 min (Figure 3D) of reaction time, respectively. As noted at 10 min, the sample possessed areas characterized by structures with a needle-like morphology but overall, it lacked uniformity since some of these needle-like motifs were aggregated together, whereas others remained as scattered, discrete entities. At 30 min, the as-synthesized sample was consistent with the formation of reasonably uniform and highly crystalline 3D nanoflowers, measuring ∼100 nm in average diameter (Figure 3C). After 90 min of reaction (Figure 3D), we observed the formation of somewhat uniform 3D nanoscale spheres, but these appeared to have an amorphous coating on their external surface. Because we were able to isolate reasonably more homogeneous and crystalline needle-like structures possessing the desired chemical composition after as little as 30 min of reaction, we chose this reaction time as an "optimized" time interval for the formation of 3D nanostructures of VS_4 using sodium orthovanadate in water.

Obviously, this reaction period was longer than that needed to produce 1D VS_4 nanorods with NMP, but this was understandable, considering that intuitively, it would take an increased reaction period to generate an inherently more complex and more sophisticated 3D hierarchical architecture. In addition, the use of water as a reaction solvent most likely lengthened the reaction time as compared with NMP itself. As mentioned previously, NMP with its larger dielectric constant is more polar than water and, therefore, possesses a relatively larger tangent factor as compared with water, meaning that NMP likely absorbed microwave energy much more readily than water[61] and therefore took less time to induce the desired reaction.

We should note that the isolated XRD pattern was somewhat ambiguous, since the singular peak could be ascribed to either VS_2 or VS_4; hence, further investigation was necessary (Figure 4A, black) to ascertain the chemical identity of our products. Acquired SEM-EDS data yielded a 1:4

https://dx.doi.org/10.1021/acssuschemeng.0c03785
ACS Sustainable Chem. Eng. 2020, 8, 16397−16412

V/S elemental ratio, consistent with the presence of VS_4 (Figure 4B). Further electron microscopy characterization enabled visualization of the resulting morphology. In effect, the isolated 3D morphology consisted of hierarchical flower-like assemblies with an average diameter of 125 ± 22 nm; this sample is highlighted as VS_4 NF-W (Figure 4C,D and Table 1).

Table 1. Summary of Average Diameters and Chemical Composition Data Derived from SEM-EDS Spectra of VS_4 3D Nanoflower Samples

sample	average diameter (in nm)	sulfur atom %	vanadium atom %	total atom %
NF-W	125 ± 22	78.9	21.0	100.0
NF-E	142 ± 33	83.6	16.4	100.0
NF-M	164 ± 28	77.7	22.3	100.0

Additional chemical characterization was achieved on VS_4 NF-W samples using XPS (Figure 5 and Table S1). Specifically, the VS_4 NF-W sample evinced V 2p peaks (Figure 5B) with a major V^{4+} signal consistent with the VS_4 formation; the presence of small V^{3+} peaks may have originated from sample drying in ethanol. Since as XPS only has a limited surface range of 10 nm, the presence of V^{3+} may have correlated with slight surface oxygenation, due to the formation of VOOH at the outer surface of the VS_4 nanoflowers.[62] The V $2p_{3/2}$ peak was observed at 516.5 eV along with a V $2p_{1/2}$ peak at 522.3 eV, correlating with data previously noted not only with the aforementioned VS_4 nanorods but also with prior literature (Figure 5B and Table S1). The S 2p region (Figure 5A) for the VS_4 NF-W sample yielded two $2p_{3/2}$ and $2p_{1/2}$ peaks at 162.4 and 164.0 eV, respectively (Table S1), consistent with the S_2^{2-} dimer formation and in line with the corresponding measurements of VS_4 nanorods. Collectively, we can assert the formation of

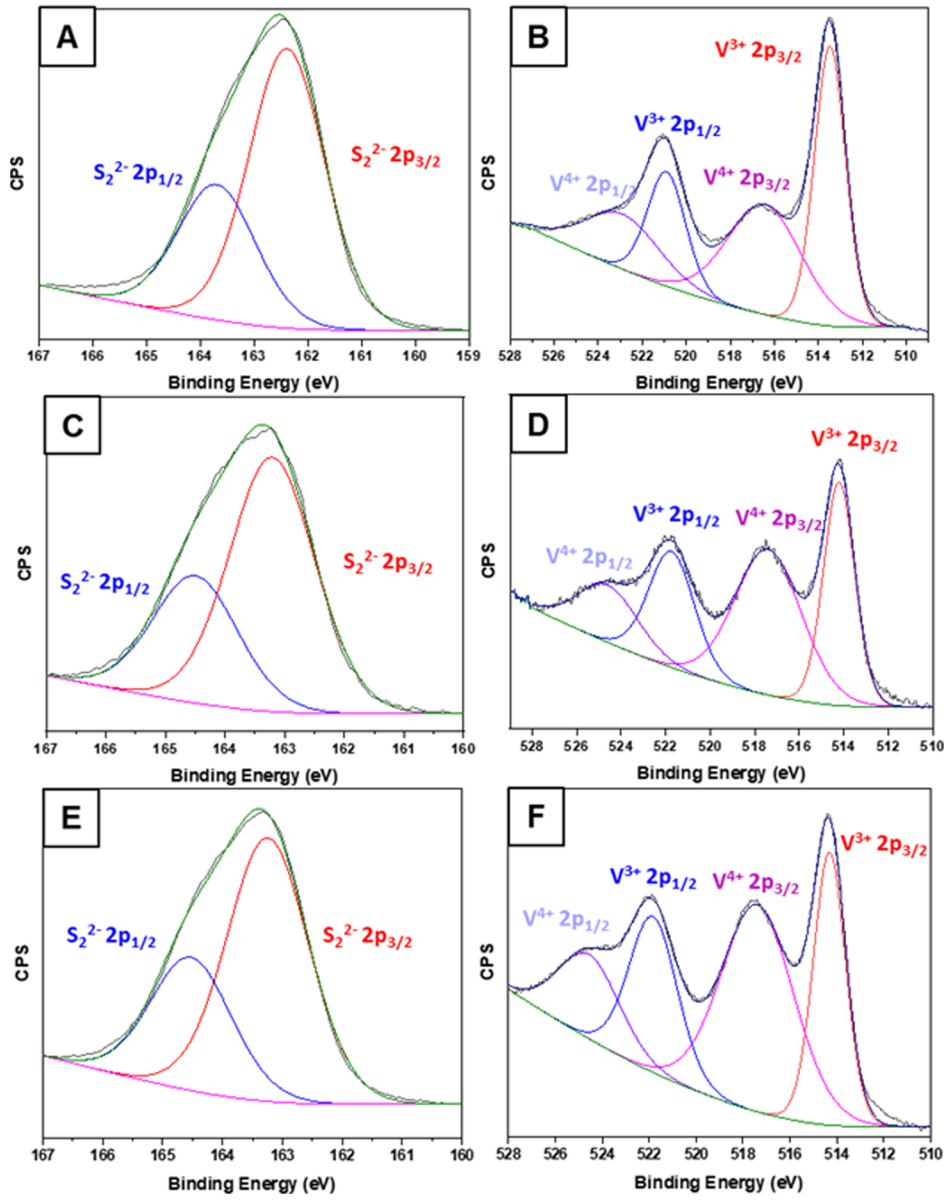

Figure 5. XPS spectra of as-obtained VS_4 3D nanoflowers: (A, B) NF-W, (C, D) NF-E, and (E, F) NF-M for (A, C, E) the S 2p region and (B, D, F) the V 2p region.

https://dx.doi.org/10.1021/acssuschemeng.0c03785
ACS Sustainable Chem. Eng. 2020, 8, 16397−16412

VS_4 through the confirmation of not only the correct V^{4+} oxidation state but also the presence of the predicted S_2^{2-} dimeric species.

Varying Solvent Conditions. Because solvent choice proved to be an effective contributor to successful VS_4 nanorod generation (Figure 2), by analogy, we also tested the role of solvent with respect to VS_4 nanoflower generation. Since the use of water worked effectively to induce the formation of a distinctive 3D nanostructure, we then tried out an ethylene−water mixture (volume ratio of 1:1) as the solvent with Na_3VO_4 and TAA as the vanadium and sulfur sources, respectively; all of the reactants were thoroughly mixed together with sonication. In a series of experiments, we ran the microwave treatment at 160 °C with different reaction times (i.e., 10, 30, and 60 min). The XRD data, as shown in Figure S10A, suggested an increasing degree of crystallinity in the as-obtained VS_4 with longer reaction times. The isolated product morphologies of VS_4 included nanoscale flowers (possessing a diameter range of less than 200 nm) and submicron-scale spherical motifs (with an average diameter of ∼600 nm), as presented in Figure S10B−D.

To explore the discrete effect of the polar solvent upon the observed crystallinity of these 3D nanoscale flower-like structures, in general, we investigated the use of other solvents, such as ethanol and methanol, in combination with water. The resulting XRD pattern obtained from synthesis with an ethanol/water mixture (sample NF-E) also matches that of pure VS_4 with the presence of two discrete peaks, and it is consistent with the prior literature (Figure 4A, red).[18] Structurally, we were able to create the desired 3D flower-like nanostructures (Figure 4E,F). Specifically, it was observed that a distinctive ethanol/water combination mixture (1.4 mL water/1 mL ethanol) resulted in the production of highly crystalline 3D nanosheet aggregates (Figure 4E,F), averaging 142 ± 33 nm in diameter per cluster (Table 1). Furthermore, HRTEM images highlight the creation of 3D nanosheet clusters; measured lattice parameters of 0.56 nm within these structures matched the (110) plane, denoting data characteristic of an expected VS_4 chemical composition (Figure S12). Further investigation was performed using SEM-EDS to ensure that VS_4 could indeed be generated without the mediation of a carbon-based template. In addition, a representative SEM-EDS spectrum (Figure S11A) established the presence of a 1:4 V to S ratio, derived from the atomic weight results obtained from the collected spectra (Table 1), thereby providing for additional corroboration that VS_4 is indeed the correct isolated composition.

We also explored a polar solvent combination involving water and methanol (sample NF-M). Using identical conditions to those utilized to fabricate VS_4 NF-E with only methanol substituted for ethanol, our analogous VS_4 NF-M samples consisted of slightly larger nanoflowers with an average diameter range of 164 ± 28 nm, as confirmed by TEM data (Figure 4G,H and Table 1). Furthermore, the chemical composition of the resulting VS_4 NF-M was corroborated by XRD (Figure 4A, blue) and verified using SEM-EDS (Figure S11B). Upon comparing the various as-synthesized 3D VS_4 nanostructures (NF-W, NF-E, and NF-M), we noted the influence and close connection of solvent choice with the resulting product size. For example, the smallest VS_4 nanoflowers were obtained from the use of water alone (NF-W), whereas the largest structures isolated derived from the utilization of a methanol: water combination (NF-M) (Table 1). This observation could correlate with the relatively higher polarity and tangent factor of methanol as compared with ethanol and water; in essence, methanol would have undergone the most rapid heating protocol. Hence, its improved reactivity would have allowed for the creation of sizeable VS_4 structures.[61]

Further characterization data were obtained on the VS_4 NF-E and NF-M samples using XPS (Figure 5C−F and Table S1). The VS_4 NF-E and NF-M samples for the V 2p region were consistent with the formation of V^{4+} associated with VS_4; as previously discussed with the VS_4 NF-W sample, slight V^{3+} impurity peaks would have been consistent with the creation of VOOH species at the external surfaces of the VS_4 nanoflowers, due to drying in air.[62] The positions of the V $2p_{3/2}$ and V $2p_{1/2}$ peaks centered at ∼516 eV (Table S1) and ∼522 eV (Figure 5D,F and Table S1), respectively, were within the experimental range of both the prior literature and our own as-prepared 1D VS_4 nanorods. In addition, the S 2p region (Figure 5C,E) for the VS_4 NF-E and NF-M nanoflowers gave rise to two peaks (i.e., $2p_{3/2}$ and $2p_{1/2}$) at ∼162.5 and 164 eV, respectively (Table S1), consistent with the S_2^{2-} dimer formation. Again, the combination of V and S XPS data supported our presumption of successful VS_4 nanoflower synthesis.

Varying Sulfur Precursor Concentration and Order of Precursor Addition. Since many of the VS_4 syntheses use a nonstoichiometric amount (i.e., an excess) of sulfur precursor,[18] specifically in the context of a molar 1 V:5 S ratio, instead of the stoichiometric molar 1 V:4 S ratio, the effect of varying sulfur concentration was also explored. Specifically, when decreasing the molar amount of thioacetamide from 5 to 4 mmol (i.e., the correct stoichiometric amount for VS_4), the resulting XRD pattern (Figure 6C, red) showed that pure VS_4 had indeed been generated. However, the corresponding experimental SEM images provided evidence for a different, unexpected morphological motif, i.e., larger VS_4 spheres (as opposed to high-surface-area, spiky flower-like assemblies) with much less apparent crystallinity (Figure 6A). These findings are consistent with those noted with other metal sulfides, wherein the impact of increasing thioacetamide (TAA) concentrations was not only to facilitate the formation of the desired nanoflower morphology but also to increase the crystallinity of the resulting product.[63] Therefore, the use of a nonstoichiometric 1 V:5 S molar ratio (i.e., excess sulfur) was necessarily essential to achieving both the preferred crystallinity and morphology.

Moreover, the order of addition of the VS_4 precursors was also explored. Many reported syntheses dissolve the sulfur precursor prior to that of the vanadium precursor. For most of our experiments, the sulfur precursor (thioacetamide) was initially dissolved in a water/ethanol solution to which the vanadium precursor (Na_3VO_4) was then added and subsequently dissolved. We tried to reverse this order. Specifically, since the vanadium precursor is readily soluble in water, we dissolved the vanadium precursor in water first and then added in ethanol to enable the subsequent dissolution of the sulfur precursor. While this procedure decreased the overall sample preparation time, the resulting experimental XRD pattern (Figure 6C, black) was not consistent with pure VS_4; in fact, visible VO_2 impurity peaks (JCPDS no. 65-7960) appeared at ∼15°. Moreover, the associated SEM image showed the presence of large micron-sized impurities, most likely correlated with the VO_2 impurity (Figure 6B).

https://dx.doi.org/10.1021/acssuschemeng.0c03785
ACS Sustainable Chem. Eng. 2020, 8, 16397−16412

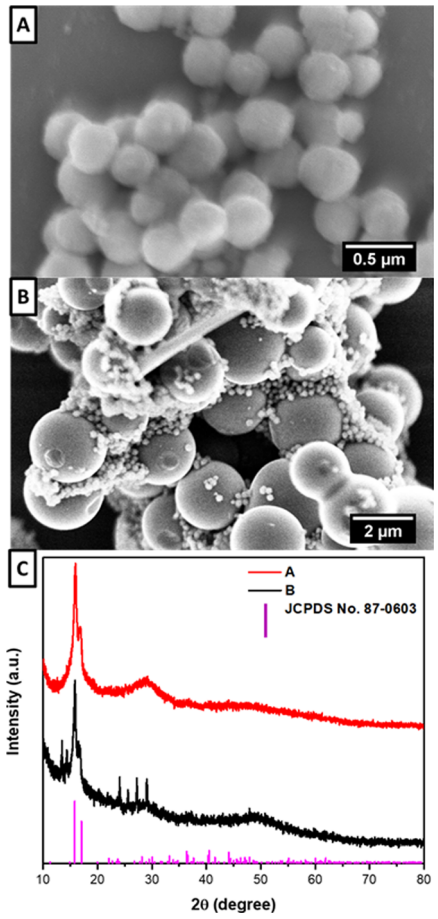

Figure 6. Probing the effect of sulfur-to-vanadium precursor ratio and order of addition. Experimental SEM images of VS_4 nanoflower-like aggregates created with (A) 1:4 molar ratio of sulfur precursor to the vanadium precursor and (B) dissolution of sodium orthovanadate in water, prior to the analogous dissolution of the sulfur precursor in the presence of a water/ethanol mixture. (C) XRD patterns of samples produced in (A) and (B), as compared with a standard VS_4 diffraction pattern.

What our findings therefore imply is that the precursor addition sequence definitely matters. Specifically, the initial dissolution of the sulfur precursor is necessary to prevent any subsequent, unwanted coordination of vanadium ions onto oxygen species present within aqueous media such as water, which would have accounted for the formation of the undesirable vanadium oxide impurities. That is, dissolving the sulfur precursor prior to adding in the vanadium precursor ensured that most, if not all, of the vanadium ions in solution coordinated with the targeted sulfur anions. Hence, the initial addition of the sulfur precursor to the water/ethanol solution was crucial in terms of not only inhibiting the production of V_xO_y impurities but also promoting the desired formation of VS_4.

Summary of Mechanistic Insights. To summarize our work on parameter control, we found that we could "optimize" our synthesis of VS_4 nanorods with respect to crystallinity and chemical composition by using a reaction temperature of 180 °C with a reaction time of 10 min. Regarding our ability to tune morphology, we noted that changing the nature of solvents and vanadium precursors yielded reproducible variations in the production of 1D VS_4 nanorod motifs. Specifically, nanorods were initially synthesized by using NMP and water mixture as the solvent; however, a mixture of nanoscale spheres and nanorods was produced when using either pure NMP or pure DMF. Further improvements, as manifested by the substitution of the vanadium precursor with Na_3VO_4 coupled with the use of a specific H_2O, H_2O/ethanol, or H_2O/methanol volume mixture, enabled the production of high-quality 3D VS_4 nanoflowers with tunable sizes from 100 to 200 nm.

Decomposition Study of VS_4 Nanorods. To probe VS_4 stability under functional conditions, we exposed our samples to environments, rich in either oxygen, water moisture, or visible light, so as to understand the underlying rationale for possible degradation routes. In Figure S13A, the sample, obtained after storing in air for several days, evinced a different coloration ("greenish" hue) as compared with a fresh sample (black powder). We can most likely attribute this change to the formation of V^{4+}- and V^{5+}-based oxides since VO_2 is blue and V_2O_5 is yellow, as suggested by the XRD pattern (Figure S13B) of the "degraded" sample. To analyze the stability of the VS_4 samples, dried VS_4 nanorod samples were stored in air under either visible irradiation (test "A") or dark conditions (test "B"). Both samples gave rise to similar color changes, even after ambient storage for about 3 weeks, suggestive of similar degradation patterns regardless of the presence of light. We found that the presence of water (and solution in general) also impacted upon the observed stability. Specifically, when VS_4 nanorods are purposely stored under moist conditions, they decayed much faster as compared with "dry" samples. As examples, we probed samples that were stored in either water or ethanol for either 1 week (test "C") or 2−3 days (test "D"), respectively. As demonstrated by XRD, these samples did not "survive" since the degree of purity lowered for both cases. By contrast, for the sample stored in a glovebox (test "E") in the absence of air and water, the VS_4 sample lasted a notably long period of time without any detectable degradation. Hence, we hypothesize that ambient storage in moist air (i.e., not in a glovebox environment) may oxidize and hydrate the exposed VS_4 over time in a process that is accelerated by the presence of either water or ethanol. These data are summarized in Table S2.

Electrochemistry. As a means of characterization for battery feasibility, electrochemical cyclic voltammetry (CV) data were obtained on various VS_4 samples. The initial pristine, as-prepared VS_4 nanorods (Figure 7A) displayed cathodic peaks at 1.95, 1.71, and 1.51 V, which can be attributed to the formation of $Li_{3+x}VS_4$. There is no apparent peak at 0.64 V to indicate the generation of an SEI layer, which we observed with our other test samples. Upon oxidation, there is a sharp anodic peak at 1.89 V and a larger peak at 2.39 V, which can be identified with the delithiation of Li_2S coupled with the formation of VS_4 or $Li_{3+x}VS_4$, respectively.[18] In the second cycle, there is only one apparent cathodic peak at 1.47 V that has shifted to a more negative potential. The evident difference between the CV and voltage profiles between the first and second cycles may be indicative of an irreversible phase transition occurring during the first reduction−oxidation process, an observation previously noted with other transition-metal sulfides.[10] Specifically, the anodic peaks in the second cycle are greatly diminished in intensity, thereby suggesting irreversibility of the process in the second cycle.

By contrast, upon annealing, the VS_4 nanorods exhibited three main cathodic peaks in the first cathodic scan (Figure 7B), situated at 1.78, 1.65, and 1.5 V. The peaks in this region

https://dx.doi.org/10.1021/acssuschemeng.0c03785
ACS Sustainable Chem. Eng. 2020, 8, 16397−16412

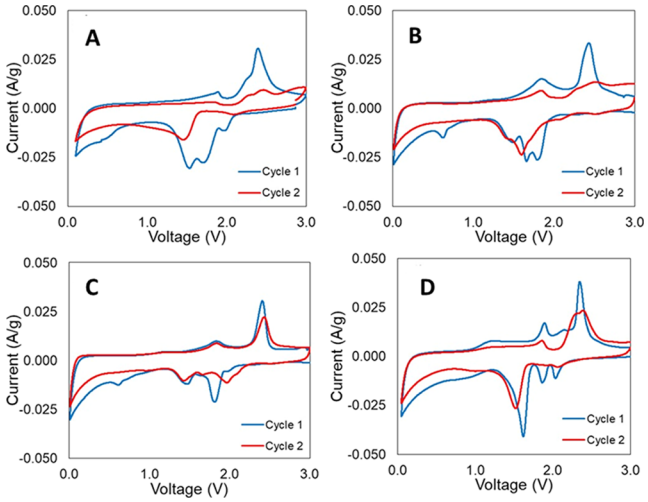

Figure 7. CVs of (A) pristine VS_4 nanorods, (B) annealed VS_4 nanorods, (C) annealed VS_4 nanorod/MWNT composites, and (D) VS_4 nanoflowers. These data sets were obtained at a 0.1 mV/s scan rate between 0.01−0.05 and 3.0 V vs Li/Li^+.

can be attributed to a likely multi-step lithiation of VS_4 to form $Li_{3+x}VS_4$. A smaller peak appears at ∼0.64 V, which had not been noted with pristine VS_4 nanorods (Figure 7A), and can be viably ascribed to a combination of (i) SEI formation, (ii) the decomposition of the electrolyte, and (iii) the reduction of $Li_{3+x}VS_4$ to Li_2S and V.[18] During the first anodic scan, peaks are present at 1.83 and 2.43 V, consistent with not only delithiation of the Li_2S at 1.83 V but also the formation of either VS_4 or $Li_{3+x}VS_4$ at 2.43 V.[18] In the second cycle, there is a cathodic peak at 1.59 V with a shoulder located at ∼1.42 V. The peak at 0.64 V disappears, consistent with the irreversible formation of the SEI layer. The observed change in the peak potential from the first scan may be explained by either a compositional change or a structural rearrangement from the previous cycle. The second anodic scan reveals a decrease in the peak current at 1.83 V, coupled with a major intensity decrease and broadening of the peak at 2.43 V. What we can state is that the addition of a physical annealing step between Figure 7A,B implies an increased sample crystallinity. It has been previously reported that higher crystallinity is conducive to a larger capacity and a more stable cycling, not only because of the likelihood of fewer defects within a thermally treated sample but also because amorphous phases tend to induce disorder and render it more difficult for Li-ion diffusion.[18] Hence, it is not surprising that there is an enhanced reversibility and stability of annealed versus pristine VS_4 nanorods.

By comparison, the CV data of the annealed VS_4 nanorod/MWNT sample (Figure 7C) show similar behavior with that of annealed VS_4 nanorods. In particular, the main cathodic peak appears at 1.81 V with smaller peaks situated at 1.48 and 1.98 V, with the SEI peak positioned at 0.64 V. Anodic peaks appear at 1.83 and 2.41 V. In the second cycle, instead of shifting to a lower potential, the cathodic peak moves to a higher potential at around 1.98 V. Zhou et al. described a similar type of behavior with their analogous VS_4 nanoparticle/MWNT structure during CV, wherein they attributed this shift to either a structural rearrangement or a chemical compositional change within their test material.[16] As had been discussed in the Introduction section, in an optimal scenario, the presence of MWNTs likely improved the conductivity, charge-transfer kinetics, and cycling stability of the resulting electrode, all of which would have led to a better cycling stability and rate capability.[24] Not surprisingly, the shift to a more positive potential may be ascribed to increased kinetics from the presence of MWNTs, which would have facilitated charge transfer to the adjoining VS_4 nanorods. In the second anodic scan, the peaks are similar to that of the first cycle, with a slight broadening in the peak at 2.41 V.

To further account for the unique electrochemical behavior of our composites, we probed their spatial organization by comparing the 3D arrangement of pristine VS_4 nanorods versus VS_4/MWNT composites through an analysis of their X-ray nanotomography scans, as shown in Figure 8. The

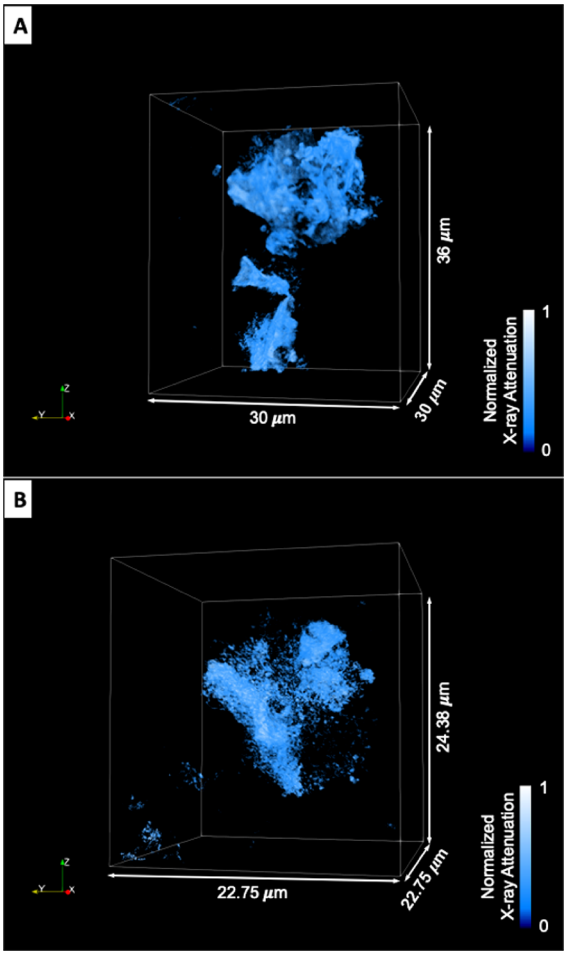

Figure 8. Reconstructed 3D X-ray nanotomography images of (A) VS_4 nanorods and (B) VS_4 nanorod/MWNT composites.

reconstructed 3D sample morphologies are shown within spatially designated regions in the shape of square boxes. According to the 3D tomography data, the VS_4/MWNT composite (Figure 8B) yielded a more homogeneous distribution as compared with pristine VS_4 alone (Figure 8A), which appeared to have evinced large aggregates within the analyzed volume. After attaching the VS_4 nanorods onto the MWNTs, VS_4 tended to grow on its underlying surface and formed a loose, winding, necklace-like structure, reflecting the directionality of the MWNT backbone. As for the pristine VS_4 nanorods, since there was no template "spine" with which to "channel" their growth, then the net result was a high degree of

https://dx.doi.org/10.1021/acssuschemeng.0c03785
ACS Sustainable Chem. Eng. 2020, 8, 16397−16412

Table 2. Summary of Different Morphologies of VS_4 Produced in This Work, Created Using Different Sets of Reaction Conditions

vanadium precursor	sulfur precursor	solvent	reaction time (min)	reaction temperature (°C)	chemical composition	morphology
$VO(acac)_2$	thioacetamide	NMP/H_2O	10	180	VS_4	uniform nanorods
$VO(acac)_2$	thioacetamide	NMP	10	180	VS_4	mixture of nanowires and spheres
$VO(acac)_2$	thioacetamide	DMF	10	180	VS_4	mixture of nanowires and spheres
$VO(acac)_2$	L-cysteine	NMP/H_2O	10	180	VS_4	flower-like structures
$VO(acac)_2$	thioacetamide	MeOH	30	160	VS_4 with $VO(acac)_2$	n/a
$VO(acac)_2$	thioacetamide	EtOH	30	160	VS_4 with $VO(acac)_2$	n/a
$VO(acac)_2$	thioacetamide	$MeOH/H_2O$	30	160	VS_4 with $VO(acac)_2$	n/a
$VO(acac)_2$	thioacetamide	$EtOH/H_2O$	30	160	VS_4 with $VO(acac)_2$	n/a
Na_3VO_4	thioacetamide	H_2O	30	160	VS_4	nanoflower-like aggregates
Na_3VO_4	thioacetamide	EG/H_2O	10	160	VS_4	flower-like structures
Na_3VO_4	thioacetamide	$EtOH/H_2O$	30	160	VS_4	nanoflower-like aggregates
Na_3VO_4	thioacetamide	$MeOH/H_2O$	30	160	VS_4	nanoflower-like aggregates

apparent and diffuse aggregation. Therefore, at a larger macroscopic level, the presence of MWNTs appears to have enabled a relatively uniform and even dispersion/packing of VS_4 nanorods, thereby limiting their aggregation and creating an overall better interconnected network, which might have more readily accommodated for volume expansion upon lithiation. Hence, these direct observations of structure may explain the improved electrochemical performance of VS_4/MWNT composites as compared with that of their pristine VS_4 analogues.

In the final set of experiments involving VS_4 nanoflowers (NF-E) (Figure 7D), we observed three distinctive cathodic peaks in the first cycle (2.02, 1.87, and 1.62 V) as opposed to the close grouping of peaks that had appeared in the other samples. These data can be attributed to VS_4 lithiation. No peak was visible at 0.64 V to indicate SEI formation, by contrast with results found with other VS_4 nanoflower samples.[18] Nonetheless, we found that peaks at 2.02 and 1.87 V disappeared completely in the second cycle, which was consistent with the performance of other VS_4 materials,[10] whereas the peak at 1.62 V shifted slightly to 1.52 V. In the first anodic scan, there are three separate peaks located at 1.90, 2.14, and 2.36 V, corresponding to the delithiation of the products, formed during the reduction. The second anodic scan highlights a decrease in the peak current with peak broadening located at 2.36 V. Again, the apparent difference between the CV first and second reduction cycles likely signified an irreversible phase transition occurring during the first reduction−oxidation process, denoting similar behavior with that of other transition-metal sulfides.[10] Nonetheless, it should be noted that the pristine nanoflowers (Figure 7D) evinced greater reversibility and electrochemical function as compared with that of pristine nanorods (Figure 7A), likely because of the increased surface area and higher porosity of the hierarchical 3D structure, which would have facilitated Li^+-ion transport and accommodated for volume changes upon charge/discharge.[18]

Summary of Electrochemical Testing. Overall, our as-prepared and unique VS_4 morphologies and compositions displayed similar groupings of peaks upon the first cathodic scan. In the literature, similar sets of peaks have been ascribed to the formation of a lithiated Li_{3+x} phase, followed by the formation of Li_2S and V.[18] Pristine nanorods (Figure 7A) and nanoflowers (Figure 7D) did not give rise to any SEI formation, whereas annealed VS_4 nanorods (Figure 7B) yielded a small peak at 0.64 V, which had been previously attributed to SEI formation. Whereas the VS_4 nanorod/MWNT composites did not experience a negative shift in potential (Figure 7C), the analogous unattached, bare VS_4 samples experienced a shift to more negative potentials during the second cathodic scan. Moreover, two prominent anodic peaks were present in all samples, coupled with a minor third peak associated with the CV of VS_4 nanoflowers (Figure 7D), all of which could be attributed to the delithiation of Li_2S and the reformation of $Li_{3+x}VS_4$. It is possible that the material does not fully revert to VS_4, thereby accounting for the difference in peaks during the second cathodic scan. We hypothesize that the compositional change discussed in the literature may be a partially lithiated version of the original VS_4 material.[16] Future work will include experiments such as but not limited to (i) annealing of VS_4 nanoflowers in addition to (ii) composite formation involving these 3D VS_4 motifs with MWNTs to further probe the resulting electrochemical behavior.

CONCLUSIONS

In this work, a facile and fast microwave-assisted method was developed to synthesize VS_4 and its associated composite heterostructures, VS_4/MWNT. We noted that pure and highly crystalline VS_4 nanorods could be generated via a 10 min reaction at 180 °C, followed by annealing at 300 °C under inert Ar conditions for 1 h. Moreover, the VS_4 morphology itself could be easily tuned by simply changing specific reaction parameters. In particular, VS_4 nanorods with average lengths of ∼318 nm and average widths of ∼77 nm could be synthesized by using a mixture of NMP and water as the solvent, whereas a combination of nanorods and nanoscale spheres could be produced by using either pure NMP or pure DMF alone.

By changing the vanadium precursor to sodium vanadate, 3D nanoflowers were synthesized using selected water: polar solvent ratios, ranging from an all-water solution (NF-W), onwards to a water: ethanol mixture (NF-E) and finally to a water/methanol combination (NF-M). These nanoflowers were noted to be highly crystalline and were found to increase in size in a deterministic fashion with increasing polarity of the solvent mixture. Further experimentation yielded insights into the mechanistic growth of the VS_4 nanoflower-like structures,

https://dx.doi.org/10.1021/acssuschemeng.0c03785
ACS Sustainable Chem. Eng. 2020, 8, 16397−16412

wherein both the molar ratio of V to S content and the order of addition of the precursors were found to play significant roles. In particular, decreasing the initial molar ratios of V to S content from a nonstoichiometric value of 1:5 to a stoichiometric molar ratio of 1:4 yielded pure VS_4. However, that protocol produced a less crystalline, spherical-like morphology. By contrast, altering the order of addition by initially adding in the vanadium precursor prior to inserting in the sulfur precursor resulted in the formation of undesirable vanadium oxide impurities. All of these different isolated morphologies coupled with their associated synthetic protocols are summarized in Table 2.

Hence, this simple microwave method not only is a new, simple, and fast method for preparing VS_4 but also is potentially generalizable as a facile means with which to modify morphology by controllably altering specific reaction parameters, which can be subsequently correlated with their associated electrochemical performance as electrode materials. In addition, the degradation of VS_4 nanorods was analyzed for the first time as well, with results suggesting that VS_4 disintegrates, when in the presence of either air, solution, or a combination of these environments. These data imply the inherent sensitivity of VS_4 with implications for their practical applicability within commercial device configurations.

From an electrochemical perspective, our VS_4 is electrochemically active and shows behavior consistent with the literature. Moreover, we found that the rational application of specific physical and chemical processing treatments, such as (i) thermal annealing to increase crystallinity, (ii) the addition of MWNTs to form conductive composites, and (iii) the evolution of morphology from 1D nanorods to more complex 3D nanoflowers, yielded distinctive effects upon the resulting electrochemistry. All of these deliberative interventions led to clear improvements, especially with respect to reversibility, as compared with pristine VS_4 nanorods alone. It is difficult if not impossible to clearly differentiate and ascertain the relative importance and/or benefits of any one mutually independent reaction variable in dictating the observed performance. No one variable is most decisive. Rather, our results are consistent with emphasizing the significance of each of these synthetic strategies, in particular, in terms of holistically assessing and improving upon the resulting stability and measured capacity of as-prepared VS_4 motifs, with implications for increasing the observed battery performance.

■ ASSOCIATED CONTENT

Supporting Information

The Supporting Information is available free of charge at https://pubs.acs.org/doi/10.1021/acssuschemeng.0c03785.

> Structural and chemical characterization results, including but not limited to XPS, XRD, SEM, SEM-EDS, and HRTEM figures, associated with analyzing the effects of various reaction parameters (including but not limited to precursors, solvents, reaction times, and reaction temperatures) on different types of as-prepared VS_4 motifs (including nanorods, nanoflowers, and MWNT-based composites), coupled with tables summarizing and quantifying acquired XPS and relevant storage data (PDF)

■ AUTHOR INFORMATION

Corresponding Author

Stanislaus S. Wong − *Department of Chemistry, State University of New York at Stony Brook, Stony Brook, New York 11794-3400, United States;* orcid.org/0000-0001-7351-0739; Email: stanislaus.wong@stonybrook.edu

Authors

Kenna L. Salvatore − *Department of Chemistry, State University of New York at Stony Brook, Stony Brook, New York 11794-3400, United States*

Sha Tan − *Department of Chemistry, State University of New York at Stony Brook, Stony Brook, New York 11794-3400, United States;* orcid.org/0000-0001-8277-893X

Christopher Tang − *Department of Materials Science and Chemical Engineering, State University of New York at Stony Brook, Stony Brook, New York 11794-2275, United States*

Joceline Gan − *Department of Chemistry, State University of New York at Stony Brook, Stony Brook, New York 11794-3400, United States*

Matthew Licht − *Department of Chemistry, State University of New York at Stony Brook, Stony Brook, New York 11794-3400, United States*

Cheng-Hung Lin − *Department of Materials Science and Chemical Engineering, State University of New York at Stony Brook, Stony Brook, New York 11794-2275, United States;* orcid.org/0000-0001-9254-9751

Xiao Tong − *Center for Functional Nanomaterials, Brookhaven National Laboratory, Upton, New York 11973, United States*

Yu-chen Karen Chen-Wiegart − *Department of Materials Science and Chemical Engineering, State University of New York at Stony Brook, Stony Brook, New York 11794-2275, United States; National Synchrotron Light Source II, Brookhaven National Laboratory, Upton, New York 11973, United States;* orcid.org/0000-0003-4445-2159

Esther S. Takeuchi − *Department of Chemistry and Department of Materials Science and Chemical Engineering, State University of New York at Stony Brook, Stony Brook, New York 11794-3400, United States; Energy Sciences Directorate, Brookhaven National Laboratory, Upton, New York 11973, United States;* orcid.org/0000-0001-8518-1047

Kenneth J. Takeuchi − *Department of Chemistry and Department of Materials Science and Chemical Engineering, State University of New York at Stony Brook, Stony Brook, New York 11794-3400, United States;* orcid.org/0000-0001-8129-444X

Amy C. Marschilok − *Department of Chemistry and Department of Materials Science and Chemical Engineering, State University of New York at Stony Brook, Stony Brook, New York 11794-3400, United States; Energy Sciences Directorate, Brookhaven National Laboratory, Upton, New York 11973, United States;* orcid.org/0000-0001-9174-0474

Complete contact information is available at: https://pubs.acs.org/10.1021/acssuschemeng.0c03785

Author Contributions

#K.L.S. and S.T. contributed equally to this work.

Notes

The authors declare no competing financial interest.

https://dx.doi.org/10.1021/acssuschemeng.0c03785
ACS Sustainable Chem. Eng. 2020, 8, 16397−16412

■ ACKNOWLEDGMENTS

All of the work described in these studies was funded as part of the Center for Mesoscale Transport Properties (m2M), an Energy Frontier Research Center supported by the U.S. Department of Energy, Office of Science, Basic Energy Sciences, under award #DE-SC0012673. Experimental research characterization was carried out in part at the Center for Functional Nanomaterials, Brookhaven National Laboratory, an Office of Science User Facility, which is supported by the U.S. Department of Energy, Office of Basic Energy Sciences, under Contract no. DE-SC0012704. This research used resources and the Full-Field X-ray imaging Beamline (FXI, 18-ID) of the National Synchrotron Light Source II, a U.S. Department of Energy (DOE) Office of Science User Facility operated for the DOE Office of Science by Brookhaven National Laboratory under Contract no. DE-SC0012704. The authors acknowledge the expert assistance of scientists working at the FXI beamline, including Mingyuan Ge, Xianghui Xiao, and Wah-Keat Lee. C.T. acknowledges the support of the National Science Foundation Graduate Research Fellowship under Grant 1839287. Any opinions, findings, and conclusions or recommendations expressed in this material are those of the authors and do not necessarily reflect the views of the National Science Foundation. E.S.T. acknowledges funding from the William and Jane Knapp Chair for Energy and the Environment.

■ REFERENCES

(1) Zhang, Q.; Uchaker, E.; Candelaria, S. L.; Cao, G. Nanomaterials for energy conversion and storage. *Chem. Soc. Rev.* **2013**, *42*, 3127−3171.

(2) Balogun, M.-S.; Huang, Y.; Qiu, W.; Yang, H.; Ji, H.; Tong, Y. Updates on the development of nanostructured transition metal nitrides for electrochemical energy storage and water splitting. *Mater. Today* **2017**, *20*, 425−451.

(3) Armand, M.; Tarascon, J. M. Building better batteries. *Nature* **2008**, *451*, 652−657.

(4) Whittingham, M. S. Ultimate Limits to Intercalation Reactions for Lithium Batteries. *Chem. Rev.* **2014**, *114*, 11414−11443.

(5) Goodenough, J. B.; Kim, Y. Challenges for Rechargeable Li Batteries. *Chem. Mater.* **2010**, *22*, 587−603.

(6) Li, L.; Cabán-Acevedo, M.; Girard, S. N.; Jin, S. High-purity iron pyrite (FeS_2) nanowires as high-capacity nanostructured cathodes for lithium-ion batteries. *Nanoscale* **2014**, *6*, 2112−2118.

(7) Jin, R.; Yang, L.; Li, G.; Chen, G. Hierarchical worm-like CoS_2 composed of ultrathin nanosheets as an anode material for lithium-ion batteries. *J. Mater. Chem. A* **2015**, *3*, 10677−10680.

(8) Xu, X.; Liu, W.; Kim, Y.; Cho, J. Nanostructured transition metal sulfides for lithium ion batteries: Progress and challenges. *Nano Today* **2014**, *9*, 604−630.

(9) Rout, C. S.; Kim, B.-H.; Xu, X.; Yang, J.; Jeong, H. Y.; Odkhuu, D.; Park, N.; Cho, J.; Shin, H. S. Synthesis and Characterization of Patronite Form of Vanadium Sulfide on Graphitic Layer. *J. Am. Chem. Soc.* **2013**, *135*, 8720−8725.

(10) Xu, X.; Jeong, S.; Rout, C. S.; Oh, P.; Ko, M.; Kim, H.; Kim, M. G.; Cao, R.; Shin, H. S.; Cho, J. Lithium reaction mechanism and high rate capability of VS_4−graphene nanocomposite as an anode material for lithium batteries. *J. Mater. Chem. A* **2014**, *2*, 10847−10853.

(11) Britto, S.; Leskes, M.; Hua, X.; Hébert, C.-A.; Shin, H. S.; Clarke, S.; Borkiewicz, O.; Chapman, K. W.; Seshadri, R.; Cho, J.; Grey, C. P. Multiple Redox Modes in the Reversible Lithiation of High-Capacity, Peierls-Distorted Vanadium Sulfide. *J. Am. Chem. Soc.* **2015**, *137*, 8499−8508.

(12) Li, Q.; Chen, Y.; He, J.; Fu, F.; Lin, J.; Zhang, W. Three-dimensional VS_4/graphene hierarchical architecture as high-capacity anode for lithium-ion batteries. *J. Alloys Compd.* **2016**, *685*, 294−299.

(13) Zhou, Y.; Li, Y.; Yang, J.; Tian, J.; Xu, H.; Yang, J.; Fan, W. Conductive Polymer-Coated VS_4 Submicrospheres As Advanced Electrode Materials in Lithium-Ion Batteries. *ACS Appl. Mater. Interfaces* **2016**, *8*, 18797−18805.

(14) Grayfer, E. D.; Pazhetnov, E. M.; Kozlova, M. N.; Artemkina, S. B.; Fedorov, V. E. Anionic Redox Chemistry in Polysulfide Electrode Materials for Rechargeable Batteries. *ChemSusChem* **2017**, *10*, 4805−4811.

(15) Wang, Q.; Rui, K.; Zhang, C.; Ma, Z.; Xu, J.; Sun, W.; Zhang, W.; Zhu, J.; Huang, W. Interlayer-Expanded Metal Sulfides on Graphene Triggered by a Molecularly Self-Promoting Process for Enhanced Lithium Ion Storage. *ACS Appl. Mater. Interfaces* **2017**, *9*, 40317−40323.

(16) Zhou, Y.; Tian, J.; Xu, H.; Yang, J.; Qian, Y. VS_4 nanoparticles rooted by a-C coated MWCNTs as an advanced anode material in lithium ion batteries. *Energy Storage Mater.* **2017**, *6*, 149−156.

(17) Wang, L.; Xue, L.; Wang, J.; Miao, L.; Chen, W.; Wan, M.; Gong, W.; Liu, Q.; Zhang, N.; Zhang, W. The effects of Fe@C nanoparticles on the lithium storage performance of VS_4 anode. *J. Alloys Compd.* **2018**, *768*, 938−943.

(18) Yang, G.; Zhang, B.; Feng, J.; Wang, H.; Ma, M.; Huang, K.; Liu, J.; Madhavi, S.; Shen, Z.; Huang, Y. High-Crystallinity Urchin-like VS_4 Anode for High-Performance Lithium-Ion Storage. *ACS Appl. Mater. Interfaces* **2018**, *10*, 14727−14734.

(19) Zhang, L.; Wei, Q.; Sun, D.; Li, N.; Ju, H.; Feng, J.; Zhu, J.; Mai, L.; Cairns, E. J.; Guo, J. Conversion reaction of vanadium sulfide electrode in the lithium-ion cell: Reversible or not reversible? *Nano Energy* **2018**, *51*, 391−399.

(20) Wang, M.; Fan, L.; Qiu, Y.; Chen, D.; Wu, X.; Zhao, C.; Cheng, J.; Wang, Y.; Zhang, N.; Sun, K. Electrochemically active separators with excellent catalytic ability toward high-performance Li−S batteries. *J. Mater. Chem. A* **2018**, *6*, 11694−11699.

(21) Wang, S.; Chen, H.; Liao, J.; Sun, Q.; Zhao, F.; Luo, J.; Lin, X.; Niu, X.; Wu, M.; Li, R.; Sun, X. Efficient Trapping and Catalytic Conversion of Polysulfides by VS_4 Nanosites for Li−S Batteries. *ACS Energy Lett.* **2019**, *4*, 755−762.

(22) Zhang, Q.; Wan, H.; Liu, G.; Ding, Z.; Mwizerwa, J. P.; Yao, X. Rational design of multi-channel continuous electronic/ionic conductive networks for room temperature vanadium tetrasulfide-based all-solid-state lithium-sulfur batteries. *Nano Energy* **2019**, *57*, 771−782.

(23) Zhu, L.; Yang, C.; Chen, Y.; Wang, J.; Wang, C.; Zhu, X. Lithium storage performance and mechanism of VS_4/rGO as an electrode material associated with lithium-sulfur batteries. *J. Alloys Compd.* **2019**, *785*, 855−861.

(24) Sun, R.; Wei, Q.; Li, Q.; Luo, W.; An, Q.; Sheng, J.; Wang, D.; Chen, W.; Mai, L. Vanadium Sulfide on Reduced Graphene Oxide Layer as a Promising Anode for Sodium Ion Battery. *ACS Appl. Mater. Interfaces* **2015**, *7*, 20902−20908.

(25) Pang, Q.; Zhao, Y.; Yu, Y.; Bian, X.; Wang, X.; Wei, Y.; Gao, Y.; Chen, G. VS_4 Nanoparticles Anchored on Graphene Sheets as a High-Rate and Stable Electrode Material for Sodium Ion Batteries. *ChemSusChem* **2018**, *11*, 735−742.

(26) Li, W.; Huang, J.; Cao, L.; Feng, L.; Yao, C. Controlled construction of 3D self-assembled VS_4 nanoarchitectures as high-performance anodes for sodium-ion batteries. *Electrochim. Acta* **2018**, *274*, 334−342.

(27) Wang, S.; Gong, F.; Yang, S.; Liao, J.; Wu, M.; Xu, Z.; Chen, C.; Yang, X.; Zhao, F.; Wang, B.; Wang, Y.; Sun, X. Graphene Oxide-Template Controlled Cuboid-Shaped High-Capacity VS_4 Nanoparticles as Anode for Sodium-Ion Batteries. *Adv. Funct. Mater.* **2018**, *28*, No. 1801806.

(28) Wang, Y.; Liu, Z.; Wang, C.; Yi, X.; Chen, R.; Ma, L.; Hu, Y.; Zhu, G.; Chen, T.; Tie, Z.; Ma, J.; Liu, J.; Jin, Z. Highly Branched VS_4 Nanodendrites with 1D Atomic-Chain Structure as a Promising Cathode Material for Long-Cycling Magnesium Batteries. *Adv. Mater.* **2018**, *30*, No. 1801806.

(29) Zhang, X.; Wang, S.; Tu, J.; Zhang, G.; Li, S.; Tian, D.; Jiao, S. Flower-like Vanadium Suflide/Reduced Graphene Oxide Composite:

https://dx.doi.org/10.1021/acssuschemeng.0c03785
ACS Sustainable Chem. Eng. 2020, 8, 16397−16412

An Energy Storage Material for Aluminum-Ion Batteries. *ChemSusChem* **2018**, *11*, 709−715.
(30) Qin, H.; Yang, Z.; Chen, L.; Chen, X.; Wang, L. A high-rate aqueous rechargeable zinc ion battery based on the VS_4@rGO nanocomposite. *J. Mater. Chem. A* **2018**, *6*, 23757−23765.
(31) Ratha, S.; Marri, S. R.; Behera, J. N.; Rout, C. S. High-Energy-Density Supercapacitors Based on Patronite/Single-Walled Carbon Nanotubes/Reduced Graphene Oxide Hybrids. *Eur. J. Inorg. Chem.* **2016**, *2016*, 259−265.
(32) Ratha, S.; Marri, S. R.; Lanzillo, N. A.; Moshkalev, S.; Nayak, S. K.; Behera, J. N.; Rout, C. S. Supercapacitors based on patronite−reduced graphene oxide hybrids: experimental and theoretical insights. *J. Mater. Chem. A* **2015**, *3*, 18874−18881.
(33) Wang, S.; Song, Y.; Ma, Y.; Zhu, Z.; Zhao, C.; Zhao, C. Attaining a high energy density of 106 Wh kg^{-1} for aqueous supercapacitor based on VS_4/rGO/CoS_2@Co electrode. *Chem. Eng. J.* **2019**, *365*, 88−98.
(34) Guo, W.; Wu, D. Facile synthesis of VS_4/graphene nanocomposites and their visible-light-driven photocatalytic water splitting activities. *Int. J. Hydrogen Energy* **2014**, *39*, 16832−16840.
(35) Lui, G.; Jiang, G.; Duan, A.; Broughton, J.; Zhang, J.; Fowler, M. W.; Yu, A. Synthesis and Characterization of Template-Free VS_4 Nanostructured Materials with Potential Application in Photocatalysis. *Ind. Eng. Chem. Res.* **2015**, *54*, 2682−2689.
(36) Cai, R.; Zhang, B.; Shi, J.; Li, M.; He, Z. Rapid Photocatalytic Decolorization of Methyl Orange under Visible Light Using VS_4/Carbon Powder Nanocomposites. *ACS Sustainable Chem. Eng.* **2017**, *5*, 7690−7699.
(37) Zhang, B.; Zou, S.; Cai, R.; Li, M.; He, Z. Highly-efficient photocatalytic disinfection of *Escherichia coli* under visible light using carbon supported Vanadium Tetrasulfide nanocomposites. *Appl. Catal., B* **2018**, *224*, 383−393.
(38) Pedersen, B.; et al. Unit Cell and Space Group of VS_4. *Acta Chem. Scand.* **1959**, *13*, 1050.
(39) Yokoyama, M.; Yoshimura, M.; Wakihara, M.; Somiya, S.; Taniguchi, M. Synthesis of vanadium sulfides under high pressure. *J. Solid State Chem.* **1985**, *60*, 182−187.
(40) Feng, X.; Wang, Y.; Muhammad, F.; Sun, F.; Tian, Y.; Zhu, G. Size, Shape, and Porosity Control of Medi-MOF-1 via Growth Modulation under Microwave Heating. *Cryst. Growth Des.* **2019**, *19*, 889−895.
(41) Gawande, M. B.; Shelke, S. N.; Zboril, R.; Varma, R. S. Microwave-Assisted Chemistry: Synthetic Applications for Rapid Assembly of Nanomaterials and Organics. *Acc. Chem. Res.* **2014**, *47*, 1338−1348.
(42) Yan, H.; Li, J.; Liu, D.; Jing, X.; Wang, D.; Meng, L. Controlled preparation of high quality WS_2 nanostructures by a microwave-assisted solvothermal method. *CrystEngComm* **2018**, *20*, 2324−2330.
(43) Sehrawat, P.; Julien, C.; Islam, S. S. Carbon nanotubes in Li-ion batteries: A review. *J. Mater. Sci. Eng. B* **2016**, *213*, 12−40.
(44) Wang, L.; Zhang, Y.; McBean, C. L.; Scofield, M. E.; Yin, J.; Marschilok, A. C.; Takeuchi, K. J.; Takeuchi, E. S.; Wong, S. S. Understanding the Effect of Preparative Approaches in the Formation of "Flower-like" $Li_4Ti_5O_{12}$—Multiwalled Carbon Nanotube Composite Motifs with Performance as High-Rate Anode Materials for Li-Ion Battery Applications. *J. Electrochem. Soc.* **2017**, *164*, A524−A534.
(45) Wu, H.; Huan, Y.; Wang, D.; Li, M.; Cheng, X.; Bai, Z.; Wu, P.; Peng, W.; Zhang, R.; Ji, Z.; Zou, M.; Yan, X. Hierarchical VS_2 Nano-Flowers as Sulfur Host for Lithium Sulfur Battery Cathodes. *J. Electrochem. Soc.* **2019**, *166*, A188−A194.
(46) Zhou, J.; Wang, L.; Yang, M.; Wu, J.; Chen, F.; Huang, W.; Han, N.; Ye, H.; Zhao, F.; Li, Y.; Li, Y. Hierarchical VS_2 Nanosheet Assemblies: A Universal Host Material for the Reversible Storage of Alkali Metal Ions. *Adv. Mater.* **2017**, *29*, No. 1702061.
(47) Li, W.; Huang, J.; Feng, L.; Cao, L.; Liu, Y.; Pan, L. VS_4 Microspheres Winded by (110)-Oriented Nanotubes with High Rate Capacities as Sodium-ion Battery Anode. *Mater. Lett.* **2018**, *230*, 105−108.
(48) Ge, M.; Coburn, D. S.; Nazaretski, E.; Xu, W.; Gofron, K.; Xu, H.; Yin, Z.; Lee, W.-K. One-minute nano-tomography using hard X-ray full-field transmission microscope. *Appl. Phys. Lett.* **2018**, *113*, No. 083109.
(49) Gürsoy, D.; De Carlo, F.; Xiao, X.; Jacobsen, C. TomoPy: a framework for the analysis of synchrotron tomographic data. *J. Synchrotron Radiat.* **2014**, *21*, 1188−1193.
(50) https://tomviz.org/ (accessed April 18, 2020).
(51) Mohan, P.; Yang, J.; Jena, A.; Suk Shin, H. VS_2/rGO hybrid nanosheets prepared by annealing of VS_4/rGO. *J. Solid State Chem.* **2015**, *224*, 82−87.
(52) Motshekga, S. C.; Pillai, S. K.; Sinha Ray, S.; Jalama, K.; Krause, R. W. M. Recent Trends in the Microwave-Assisted Synthesis of Metal Oxide Nanoparticles Supported on Carbon Nanotubes and Their Applications. *J. Nanomater.* **2012**, *2012*, No. 691503.
(53) Xiang, W.; Yang, Y.; Yang, J.; Yuan, H.; An, J.; Wei, J.; Liu, X. Surfactant and thioacetamide-assisted reflux synthesis of Bi_2S_3 nanowires. *J. Mater. Res.* **2014**, *29*, 2272−2287.
(54) Hu, H.; Wang, J.; Deng, C.; Niu, C.; Le, H. Microwave-assisted controllable synthesis of hierarchical CuS nanospheres displaying fast and efficient photocatalytic activities. *J. Mater. Sci.* **2018**, *53*, 14250−14261.
(55) Li, F.; Bi, W.; Kong, T.; Wang, C.; Li, Z.; Huang, X. Effect of sulfur sources on the crystal structure, morphology and luminescence of CdS nanocrystals prepared by a solvothermal method. *J. Alloys Compd.* **2009**, *479*, 707−710.
(56) Esmaeili, E.; Sabet, M.; Salavati-Niasari, M.; Zarghami, Z.; Bagheri, S. Effect of Sulfur Source on Cadmium Sulfide Nanostructures Morphologies via Simple Hydrothermal Route. *J. Cluster Sci.* **2016**, *27*, 351−360.
(57) Weiss, I. M.; Muth, C.; Drumm, R.; Kirchner, H. O. K. Thermal decomposition of the amino acids glycine, cysteine, aspartic acid, asparagine, glutamic acid, glutamine, arginine and histidine. *BMC Biophys.* **2018**, *11*, No. 2.
(58) Ming, F.; Liang, H.; Lei, Y.; Zhang, W.; Alshareef, H. N. Solution synthesis of VSe_2 nanosheets and their alkali metal ion storage performance. *Nano Energy* **2018**, *53*, 11−16.
(59) Rantho, M. N.; Madito, M. J.; Ochai-Ejeh, F. O.; Manyala, N. Asymmetric supercapacitor based on vanadium disulfide nanosheets as a cathode and carbonized iron cations adsorbed onto polyaniline as an anode. *Electrochim. Acta* **2018**, *260*, 11−23.
(60) Yin, X.; Cai, J.; Feng, H.; Wu, Z.; Zou, J.; Cai, Q. A novel VS_2 nanosheet-based biosensor for rapid fluorescence detection of cytochrome c. *New J. Chem.* **2015**, *39*, 1892−1898.
(61) Zhu, Y.-J.; Chen, F. Microwave-Assisted Preparation of Inorganic Nanostructures in Liquid Phase. *Chem. Rev.* **2014**, *114*, 6462−6555.
(62) Li, W.; Huang, J.; Feng, L.; Cao, L.; Feng, Y.; Wang, H.; Li, J.; Yao, C. Facile in situ synthesis of crystalline VOOH-coated VS_2 microflowers with superior sodium storage performance. *J. Mater. Chem. A* **2017**, *5*, 20217−20227.
(63) Jin, Z.; Liu, Y.; Hao, X. Self-assembly of zinc cadmium sulfide nanorods into nanoflowers with enhanced photocatalytic hydrogen production activity. *J. Colloid Interface Sci.* **2020**, *567*, 357−368.

https://dx.doi.org/10.1021/acssuschemeng.0c03785
ACS Sustainable Chem. Eng. 2020, 8, 16397−16412